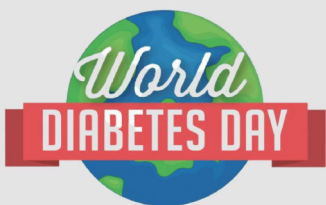


CHINA CDC WEEKLY




中国疾病预防控制中心周报



November 14, 2022

415 MILLION
people worldwide are living with diabetes.

In 2040
MORE THAN HALF A BILLION
will have diabetes.



Methods and Applications

Isolation and Characterization of Monkeypox Virus
from the First Case of Monkeypox — Chongqing
Municipality, China, 2022 1019

Epidemic Surveillance of Influenza Infections:
A Network-Free Strategy — Hong Kong
Special Administrative Region,
China, 2008–2011 1025

Uncovering the Impact of Control Strategies on
the Transmission Pattern of SARS-CoV-2
— Ruili City, Yunnan Province, China,
February–March 2022 1032

Outbreak Reports

An Outbreak of SARS-CoV-2 Omicron Subvariant
BA.2.76 in an Outdoor Park — Chongqing
Municipality, China, August 2022 1039



ISSN 2096-7071



Editorial Board

Founding Editor-in-Chief George F. Gao

Editor-in-Chief Hongbing Shen

Deputy Editor-in-Chief Liming Li Gabriel M Leung Zijian Feng

Executive Editor Feng Tan

Members of the Editorial Board

Xi Chen (USA)	Xiangsheng Chen	Xiaoyou Chen	Zhuo Chen (USA)
Xianbin Cong	Gangqiang Ding	Xiaoping Dong	Mengjie Han
Guangxue He	Zhongwei Jia	Xi Jin	Biao Kan
Haidong Kan	Qun Li	Tao Li	Zhenjun Li
Zhongjie Li	Min Liu	Qiyong Liu	Jinxing Lu
Huiming Luo	Huilai Ma	Jiaqi Ma	Jun Ma
Ron Moolenaar (USA)	Daxin Ni	Lance Rodewald (USA)	RJ Simonds (USA)
Ruitai Shao	Yiming Shao	Xiaoming Shi	Yuelong Shu
Xu Su	Xuemei Su	Chengye Sun	Dianjun Sun
Hongqiang Sun	Quanfu Sun	Xin Sun	Jinling Tang
Kanglin Wan	Huaqing Wang	Linhong Wang	Guizhen Wu
Jing Wu	Weiping Wu	Xifeng Wu (USA)	Yongning Wu
Zunyou Wu	Lin Xiao	Fujie Xu (USA)	Wenbo Xu
Hong Yan	Hongyan Yao	Zundong Yin	Hongjie Yu
Shicheng Yu	Xuejie Yu (USA)	Jianzhong Zhang	Liubo Zhang
Rong Zhang	Tiemei Zhang	Wenhua Zhao	Yanlin Zhao
Xiaoying Zheng	Zhijie Zheng (USA)	Maigeng Zhou	Xiaonong Zhou

Advisory Board

Director of the Advisory Board Jiang Lu

Vice-Director of the Advisory Board Yu Wang Jianjun Liu Jun Yan

Members of the Advisory Board

Chen Fu	Gauden Galea (Malta)	Dongfeng Gu	Qing Gu
Yan Guo	Ailan Li	Jiafa Liu	Peilong Liu
Yuanli Liu	Kai Lu	Roberta Ness (USA)	Guang Ning
Minghui Ren	Chen Wang	Hua Wang	Kean Wang
Xiaoqi Wang	Zijun Wang	Fan Wu	Xianping Wu
Jingjing Xi	Jianguo Xu	Gonghuan Yang	Tilahun Yilma (USA)
Guang Zeng	Xiaopeng Zeng	Yonghui Zhang	Bin Zou

Editorial Office

Directing Editor Feng Tan

Managing Editors Lijie Zhang

Senior Scientific Editors Ning Wang

Scientific Editors Weihong Chen

Meng Wang

Yu Chen

Ruotao Wang

Xudong Li

Xi Xu

Peter Hao (USA)

Shicheng Yu

Nankun Liu

Qing Yue

Qian Zhu

Liuying Tang

Ying Zhang

Methods and Applications

Isolation and Characterization of Monkeypox Virus from the First Case of Monkeypox — Chongqing Municipality, China, 2022

Baoying Huang^{1,✉}; Hua Zhao^{2,✉}; Jingdong Song¹; Li Zhao¹; Yao Deng¹; Wen Wang¹; Roujian Lu¹; Wenling Wang¹; Jiao Ren¹; Fei Ye¹; Houwen Tian¹; Guizhen Wu¹; Hua Ling^{2,✉}; Wenjie Tan^{1,✉}

ABSTRACT

Introduction: The first imported case of monkeypox (MPX) from the mainland of China was reported in September 2022. Herein, the study reports the isolation and characterization of MPX virus (MPXV) in this case.

Methods: Clinical specimens including skin blister fluid, oropharyngeal and nasopharyngeal swabs, and blood were collected and inoculated onto Vero cells. The isolated virus was identified as MPXV using quantitative polymerase chain reaction (qPCR), cytopathic effects (CPEs), immunofluorescence assay (IFA) and transmission electron microscopy (TEM). Plaque assays were employed to quantify infectious plaque-forming units (PFUs). The plaque reduction neutralization test (PRNT) was developed to determine the neutralizing antibody (nAb) against MPXV.

Results: MPXV replication was confirmed with qPCR. Typical CPEs were observed 48 h post-incubation. The isolated virus was named MPXV-B.1-China-C-Tan-CQ01. IFA showed that MPXV reacted with serum of MPX case. *Orthopoxvirus* morphology was observed using TEM. The virus titer increased to $>10^6$ PFU/mL after three passages. The serum PRNT 50% neutralization titer (NT₅₀) was 35 for the MPX patient 6 days after symptom onset.

Discussion: The study successfully isolated the first MPXV strain in the mainland of China, MPXV-B.1-China-C-Tan-CQ01. Infectious titration and PRNT methods have been developed. The study provides key resources and technical platforms for further research as well as anti-viral drug and vaccine development against MPX.

Monkeypox (MPX) is an emerging zoonotic disease caused by the MPX virus (MPXV), which is recognized as the most important *Orthopoxvirus* infection in

humans in the smallpox post-eradication era (1). The unexpected increase in human MPX cases in non-endemic countries raises concerns regarding a novel global public health threat (2). Between January 1 and November 10, 2022, a cumulative total of 79,151 laboratory-confirmed cases of MPX and 49 related deaths were reported to the World Health Organization by 110 countries or areas worldwide (3).

The first imported case of MPX in the mainland of China was confirmed on September 16, 2022, in a 29-year-old salesman of Chinese nationality who visited Germany (4). On September 9, the patient had a dry and itchy throat, a fever, and red rashes and pustules displayed on the right thigh. Clinical manifestations were reported, and complete genomes of the MPXV from clinical samples suggest that the MPXV strain in this case belongs to the B.1 branch of the West African lineage (4). The response to this public health emergency must include rapid isolation and identification of MPXV and development of novel assays for MPXV (5). To date, MPXV isolation and characterization have not been reported in the mainland of China. Additionally, limited information is available regarding a plaque assay for an infectious titration of MPXV and a plaque reduction neutralization test (PRNT) for MPXV-neutralizing antibody (nAb) detection on the basis of the MPXV-B.1 strains of the current epidemic.

In this study, the isolation and characteristics of MPXV in the first imported case of MPX in the mainland of China are reported. A plaque assay for MPXV infectious titration and a PRNT for MPXV nAb detection were developed.

METHODS

For virus isolation, clinical specimens including skin blister fluid, oropharyngeal and nasopharyngeal swabs, and blood were collected 6 days after symptom onset and sent to the National Institute for Viral Disease

Control and Prevention, China CDC. MPXV isolation was performed in biosafety level 3 laboratories on Vero cells. The specimens were diluted at a 1:5 ratio with culture medium, which contained 2% fetal bovine serum-Modified Eagle's Medium (FBS-MEM) and 1% antibiotics (penicillin 5,000 IU/mL, streptomycin 2,500 µg/mL, and amphotericin B 10 µg/mL, brief as PSA), treated samples were kept at 25 °C for 30 min and inoculated onto Vero cells. After incubation for 6 h at 37 °C in 5% CO₂, the supernatant was replaced with fresh medium. Cytopathic effect (CPE) appearance was observed daily.

A quantitative real-time polymerase chain reaction (qPCR) assay was conducted to confirm virus replication. Cell supernatants or lysates were collected and qPCR of MPXV was performed as reported previously (6).

For an indirect immunofluorescence assay, Vero cells were grown overnight in 8-well plates until 80% confluence and infected with the first passage of MPXV isolate. The cells were fixed with 4% paraformaldehyde 48 h post-infection, rinsed twice with phosphate-buffered saline (PBS), permeabilized with PBS containing 0.05% Triton X-100 (PBST) for 10 min, and blocked in PBST containing 2% goat serum for 30 min. After three washes, the cells were incubated with serum from the MPX case and diluted to 1:100 for 1 h at 37 °C and then incubated with the FITC-labelled anti-human immunoglobulin G diluted to 1:200, stained with 4',6-diamidino-2-phenylindole (DAPI) for 5 min, and were finally examined using the Olympus IX73 inverted fluorescence microscope.

MPXV morphologic features were determined by transmission electron microscopy assays. For the negative staining of virus particles in supernatant, the samples were enriched by ultracentrifugation and absorbed on film-coated grids, following staining with 1% PTA. For the ultrathin section sample, cell pellets were collected 48 h post infection, fixed with 2.5% paraformaldehyde-2% glutaraldehyde in 0.1 mol/L cacodylate buffer (pH 7.4) and 1% osmium tetroxide, respectively, following dehydration, infiltration with epoxy resin and polymerization. Ultrathin sections (60–80 nm) were cut with an ultramicrotome from the resin block embedded with samples and stained with uranyl acetate and lead citrate. Finally, the grids and stained sections were observed and photographs were taken under a Tecnai 12 transmission electron microscope (FEI Co., USA) at 120 kV.

Plaque assays were developed to quantify the infectious virus titer. The Vero cells were seeded on

12-well plates overnight. Ten-fold serial dilutions were performed in MEM medium containing 2% FBS and 1% antibiotics of PSA. 400 µL was used per well to infect a monolayer of Vero cells. 72 to 96 h later, the cells were fixed with 4% paraformaldehyde and stained with crystal violet. Plaque forming units (PFUs) per mL were calculated on the basis of the number of plaques multiplied by the dilution factor.

To identify the nAb induced after MPXV infection, a PRNT assay based on MPXV-B.1-China-C-Tan-CQ01 was developed. The Vero cells were seeded in 12-well. Sera were collected from the patient with MPX on day 6 after symptom onset and from two healthy 30-year-old individuals as controls, inactivated for 30 min at 56 °C, diluted in 1:20 at the beginning, and subsequently serially two folds diluted. MPXV stock (100 PFU) was added. The virus-serum mix was then incubated at 37 °C for 1 h and added to the Vero cells. The Vero cells were incubated for 96 h, fixed with 4% paraformaldehyde and stained with crystal violet.

RESULTS

Swabs from the skin lesion, oropharynx, nasopharynx, and whole blood samples were used for viral isolation in the Vero cells. Viral replication was confirmed by qPCR assay based on conserved *F3L* genes that specifically detect MPXV with DNA from cell cultures collected at 48, 96, 120, and 144 h after inoculation (Table 1). The cycle threshold (Ct) values for the nasopharyngeal swabs and blood incubations were negative at 48 h and 144 h. In contrast, for the blister fluid swab inoculation, Ct values of 27.88, 19.05, and 18.15 were detected at 48 h, 96 h, and 120 h after the inoculation. For the oropharyngeal swab inoculation, Ct values were detected as 31.00, 27.28, and 25.68 at 48 h, 96 h, and 144 h, respectively. These results indicated that MPXV replicated in the blister fluid and oropharyngeal incubation.

The virus-induced changes in CPE-related cell morphology were observed daily. The nasopharyngeal and blood-incubated cells were CPE-negative. In contrast, CPEs were observed within 48 h for the skin blister fluid-incubated cells, exhibiting cell rounding, detachment, or even death (Figure 1A). The degree of visible damage to the cells increased at 72 h, 96 h, 120 h, and 144 h, resulting in >85% CPEs (Table 1). Meanwhile, minor CPEs were also observed after 48 h for the oropharyngeal incubated cells, resulting in <20% CPEs at 144 h post-incubation (Table 1).

TABLE 1. Detection of monkeypox virus (MPXV) DNA using quantitative real-time polymerase chain reaction in Vero cell cultures with different specimens from the MPX case.

Specimen	Ct values*					CPEs at harvest time	MPXV isolation
	Clinical sample	48 h	96 h	120 h	144 h		
Blister fluid swab	20.76	27.88	19.05	18.15 [†]	ND	++++	Positive
Oropharyngeal swab	27.81	31.00	27.28	ND	25.68 [†]	+	Positive
Nasopharyngeal swab	31.00	ND	ND	ND	ND [†]	-	Negative
Blood	33.65	ND	ND	ND	ND [†]	-	Negative

Note: CPEs: -, Negative or no CPEs; +, 0–25%; ++, 25%–50%; +++, 50%–75%; +++, 75%–100%.
Abbreviation: MPXV=monkeypox virus; qPCR=quantitative real-time polymerase chain reaction; ND=not determined; CPEs=cytopathic effects; Ct=cycle threshold.
* For the blister fluid swab, viral DNAs from the supernatant of 48 h and 96 h were detected, while DNA from cell lysates of 120 h was detected. For the oropharyngeal swab, nasopharyngeal swab and blood samples, viral DNAs from the supernatant of 48 h, 96 h, 120 h were detected, while DNA from cell lysates of 144 h was detected.
[†] Harvest cell lysate.

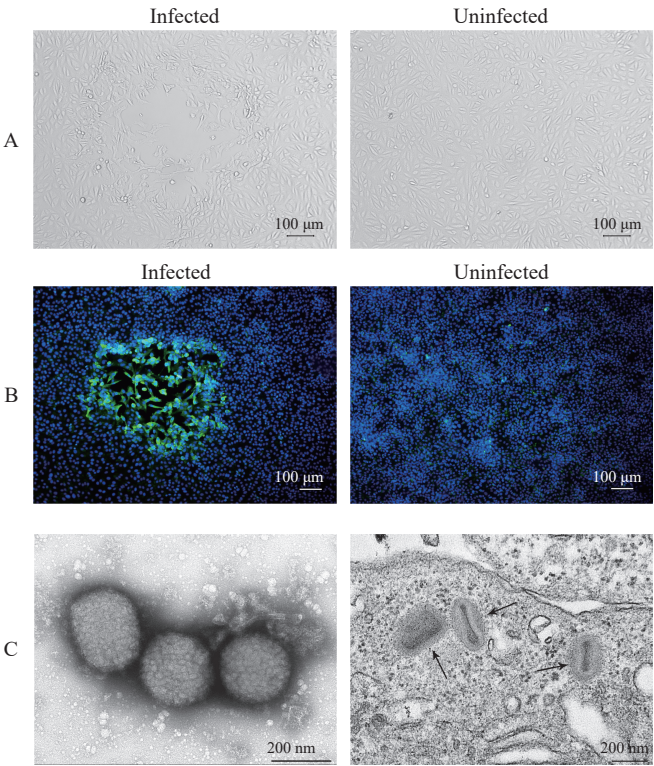


FIGURE 1. Characterization of MPXV-B.1-China-C-Tan-CQ01 in the Vero cell. (A) Cytopathic effects of monkeypox virus (MPXV) in the Vero cell; (B) Immunofluorescence analysis of Vero cell infected or uninfected with MPXV-B.1-China-C-Tan-CQ01 using the serum of the MPX case; (C) Transmission electron microscopy micrographs of MPXV.
Note: In panel A, the typical cytopathic effects are observed in the Vero cells 48 h after the first passage, thereby exhibiting cell detaching and rounding. In panel B, the nuclei were stained with DAPI (blue), while the MPXV infected cell showed green fluorescence. In panel C, the left panel showed the negative staining of purified MPXV particles with a typical brick shape observed in a diameter that varies between 200 nm and 300 nm and irregular tubular strips on the surface. The right panel showed the ultrathin section of MPXV infected Vero cell and mature virus particles in cytoplasm that show typical morphology including a dumbbell shaped core and the outer membrane on longitudinal orientation.
Abbreviation: MPXV=monkeypox virus; MPX=monkeypox; DAPI=4'6-diamidino-2-phenylindole.

Immunofluorescence assay with the patient's serum was performed to confirm MPXV antigen expression, which showed the infected foci, visualized with green fluorescence in the cell, reacted with the serum of the

patient with MPX (Figure 1B). IFA with anti-rabbit antibody against orthopoxviruses was also positive around the infected foci (data not shown).

Negative stained virus particles present a typical

brick shape about 200 nm × 200 nm × 250 nm in size with irregular tubular strips on the surface. On sections, mature virus particles in cytoplasm show typical morphology including a dumbbell-shaped core and the outer membrane on longitudinal orientation (Figure 1C).

Plaque assays indicated that the infectious MPXV titers in the first passage of blister fluid or oropharyngeal swab incubation were 6×10^4 PFU/mL and 10 PFU/mL, increased to 1×10^5 PFU/mL and 1×10^4 PFU/mL for the second passage, and to $>10^6$ PFU/mL after the third passage (Figure 2A).

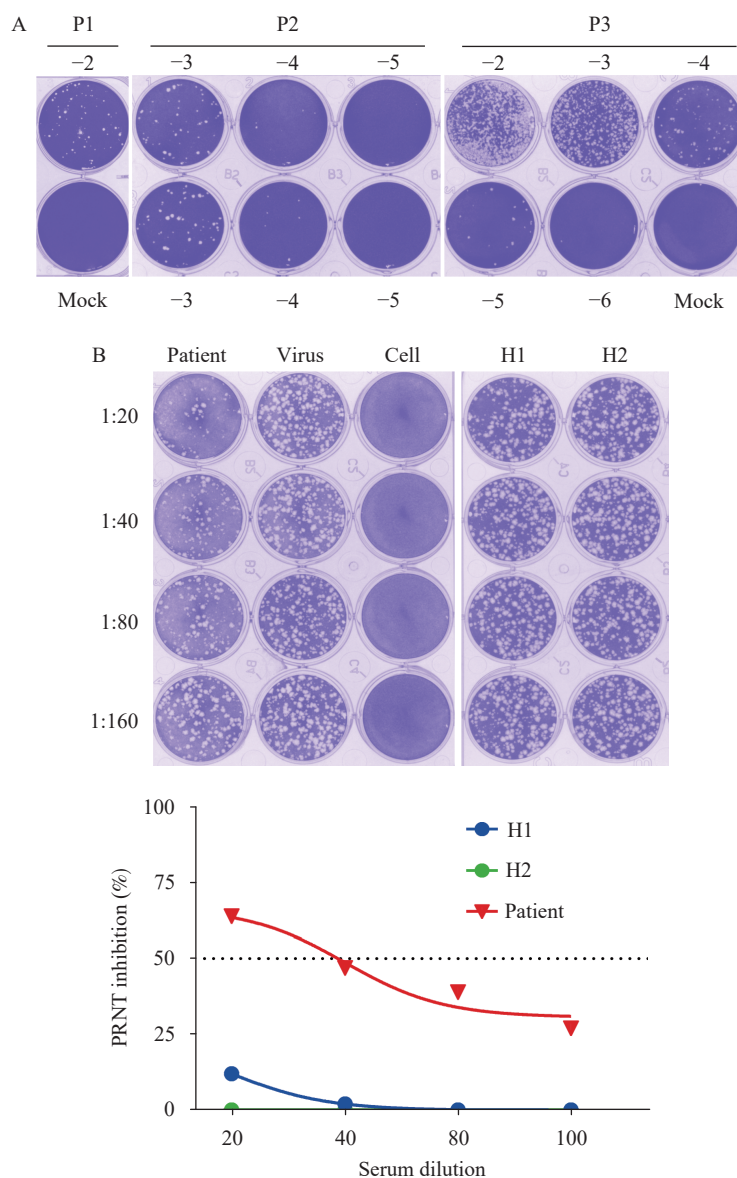


FIGURE 2. Plaque assays and PRNT based on MPXV-B.1-China-C-Tan-CQ01. (A) Quantification of infectious monkeypox virus from clinical samples (the first passage of isolation, P1, to the third passage of isolation, P3, using plaque assay). (B) Plaque reduction neutralization test to detect neutralizing antibodies (nAb) against MPXV in the serum of the MPX case (patient) and two 30-year-old healthy donors (H1 and H2).

Note: In panel A, the plates are fixed and stained with crystal violet 72 h to 96 h post-infection. Representative plates for the MPXV titration from blister fluid are shown. Plaques for P1 with a dilution of 10^{-2} (-2) and mock, for P2 with a dilution from 10^{-3} to 10^{-5} (-3, -4, -5) in double well, and for P3 with a dilution from 10^{-2} to 10^{-6} (-2, -3, -4, -5, -6) and mock are all shown. In panel B, the representative plate and neutralization curves are presented.

Abbreviation: MPXV=monkeypox virus; MPX=monkeypox; P1=the first passage of isolation; P2=the second passage of isolation; P3=the third passage of isolation; PRNT=The plaque reduction neutralization test; nAb=the neutralizing antibody; H1=healthy donor 1; H2=healthy donor 2.

A PRNT in the Vero cells with the MPXV-B.1-China-C-Tan-CQ01 was established. Serum 50% neutralization titer (NT₅₀) was detected as 35 for the MPXV case 6 days after symptom onset, while negative for the 30-year-old healthy donors (Figure 2B).

DISCUSSION

In this study, the isolation and characteristics of MPXV from the first imported MPX case in the mainland of China in 2022, named MPXV-B.1-China-C-Tan-CQ01, were reported. Based on a review of current literature, this is the first reported MPXV isolate in the mainland of China. Additionally, MPXV replication using qPCR, CPEs, and the morphological features in the Vero cells were characterized. Furthermore, novel plaque assays and PRNT were developed with the MPXV-B.1-China-C-Tan-CQ01 to quantify the infectious MPXV and nAb titer in the MPX case.

Replication-competent MPXV isolated from skin lesion swabs, oropharyngeal swabs, anal swabs, urethral swabs, and semen has been reported previously (5,7–11). However, MPXV isolation using oropharyngeal or nasopharyngeal swabs was rarely reported (12–13). Interestingly, even in the absence of oral lesions in the patient, replication-competent MPXV was also isolated from the oropharyngeal swabs in the study. This is indicative of a sufficient infectious virus presenting in the oropharyngeal site, leading to possible passage by oral droplets and contact. The results support the notion of the high prevalence of oropharyngeal and perioral lesions in the current MPX outbreak.

Current knowledge is limited to MPXV shedding and the correlation between the detected Ct value and infectious MPXV load in clinical specimens. A previous report indicated that MPXV DNA levels correlated with infectivity in clinical samples and defined a threshold (Ct ≥ 35 ; viral DNA $\leq 4,300$ copies/mL) that predicts poorly infectious specimens (14). The study measured the infectious potential of the first passages of virus isolation, with a Ct value of 20.76 for the skin blister fluid swab, the infectious MPXV was 6×10^4 PFU/mL. With a Ct value of 27.81 for the oropharyngeal swabs, the infectious MPXV was 10 PFU/mL. A clear correlation between the Ct value and virus isolation needs to be investigated in further studies, with more samples collected to represent different disease course times and body fluids.

Neutralization assays are often used to detect nAbs and determine a possible protective antibody titer after infection or vaccination. To date, data on nAbs in vaccinated individuals or MPXV-infected cases against MPX are rare. Herein, the study described a PRNT assay based on MPXV-B.1-China-C-Tan-CQ01 and detected MPXV-nAbs in the patient's serum collected on day 6 after symptom onset. As the patient was 29 years old, there was no smallpox vaccination history, and the results indicated that MPXV-infected individuals could rapidly induce nAb (<2 weeks). The PRNT described in the study is able to monitor the neutralizing immune response to MPXV and determine whether the nAb induced by historic smallpox vaccination is cross-reactive with MPXV.

In summary, the first MPXV strain in the mainland of China, named MPXV-B.1-China-C-Tan-CQ01 and representative of the current epidemic MPXV B.1 clade, was isolated. Characterization of the CPEs, replication, and morphologic features of MPXV B.1 improves collective understanding of the current MPX outbreak and its control. The novel plaque assay and PRNT developed in this study will pave the way for further research on MPXV as well as the development of anti-viral drugs and vaccines against the MPX epidemic.

Conflicts of interest: No conflicts of interest.

Funding: Supported by the National Key Research and Development Program of China (2022YFC2304100, 2022YFC2303401, 2021YFA1201003, 2016YFD0500301, 2020YFC0840900, 2021YFC0863300) and the Beijing Science and Technology Plan (Z211100002521017, Z211100002521015).

doi: 10.46234/ccdcw2022.206

Corresponding authors: Hua Ling, linghuax@163.com; Wenjie Tan, tanwj@ivdc.chinacdc.cn.

¹ Key Laboratory of Biosafety, National Health and Family Planning Commission, National Institute for Viral Disease Control and Prevention, Chinese Center for Disease Control and Prevention, Beijing Municipality, China; ² Chongqing Center for Disease Control and Prevention, Chongqing Municipal Key Laboratory for High Pathogenic Microbes, Chongqing Municipality, China.

[§] Joint first authors.

Submitted: November 01, 2022; Accepted: November 14, 2022

REFERENCES

1. Tan WJ, Gao GF. Neglected zoonotic monkeypox in Africa but now back in the spotlight worldwide. *China CDC Wkly* 2022;4(38):847–8. <http://dx.doi.org/10.46234/ccdcw2022.166>.
2. Taylor L. Monkeypox: WHO declares a public health emergency of international concern. *BMJ* 2022;378:o1874. <http://dx.doi.org/10.1136/bmj.o1874>.

3. World Health Organization. Multi-country monkeypox outbreak: situation update. 2022. <https://www.who.int/emergencies/disease-outbreak-news/item/2022-DON396>. [2022-11-2].
4. Zhao H, Wang WL, Zhao L, Ye S, Song JD, Lu RJ, et al. The first imported case of monkeypox in the mainland of China — Chongqing municipality, China, September 16, 2022. *China CDC Wkly* 2022;4(38):853 – 4. <http://dx.doi.org/10.46234/ccdcw2022.175>.
5. Lum FM, Torres-Ruesta A, Tay MZ, Lin RTP, Lye DC, Rénia L, et al. Monkeypox: disease epidemiology, host immunity and clinical interventions. *Nat Rev Immunol* 2022;22(10):597 – 613. <http://dx.doi.org/10.1038/s41577-022-00775-4>.
6. Zhou WM, Tan WJ, Zheng N, Zhang LL, Wang HJ, Ruan L. Rapid detection and differentiation of smallpox or monkeypox virus infection by real-time PCR assay. *Lett Biotechnol* 2006;17(5):703 – 6. <http://dx.doi.org/10.3969/j.issn.1009-0002.2006.05.006>. (In Chinese).
7. Thornhill JP, Barkati S, Walmsley S, Rockstroh J, Antinori A, Harrison LB, et al. Monkeypox virus infection in humans across 16 countries - April-June 2022. *N Engl J Med* 2022;387(8):679 – 91. <http://dx.doi.org/10.1056/NEJMoa2207323>.
8. Colavita F, Antinori A, Nicastrì E, Focosi D, Girardi E, Vaia F, et al. Monkeypox virus in human body sites and fluids: evidence for transmission. *Lancet Infect Dis* 2022. [http://dx.doi.org/10.1016/S1473-3099\(22\)00639-9](http://dx.doi.org/10.1016/S1473-3099(22)00639-9).
9. Peiró-Mestres A, Fuertes I, Camprubí-Ferrer D, Marcos MÁ, Vilella A, Navarro M, et al. Frequent detection of monkeypox virus DNA in saliva, semen, and other clinical samples from 12 patients, Barcelona, Spain, May to June 2022. *Euro Surveill* 2022;27(28):2200503. <http://dx.doi.org/10.2807/1560-7917.ES.2022.27.28.2200503>.
10. Noe S, Zange S, Seilmaier M, Antwerpen MH, Fenzl T, Schneider J, et al. Clinical and virological features of first human monkeypox cases in Germany. *Infection* 2022. <http://dx.doi.org/10.1007/s15010-022-01874-z>.
11. Lapa D, Carletti F, Mazzotta V, Matusali G, Pinnetti C, Meschi S, et al. Monkeypox virus isolation from a semen sample collected in the early phase of infection in a patient with prolonged seminal viral shedding. *Lancet Infect Dis* 2022;22(9):1267 – 9. [http://dx.doi.org/10.1016/S1473-3099\(22\)00513-8](http://dx.doi.org/10.1016/S1473-3099(22)00513-8).
12. Kim JW, Lee M, Shin H, Choi CH, Choi MM, Kim JW, et al. Isolation and identification of monkeypox virus MPXV-ROK-P1-2022 from the first case in the Republic of Korea. *Osong Public Health Res Perspect* 2022;13(4):308 – 11. <http://dx.doi.org/10.24171/j.phrp.2022.0232>.
13. Moschese D, Pozza G, Mileto D, Giacomelli A, Cutrera M, Cossu MV, et al. Isolation of viable monkeypox virus from anal and urethral swabs, Italy, May to July 2022. *Euro Surveill* 2022;27(36):2200675. <http://dx.doi.org/10.2807/1560-7917.ES.2022.27.36.2200675>.
14. Paran N, Yahalom-Ronen Y, Shifman O, Lazar S, Ben-Ami R, Yakubovsky M, et al. Monkeypox DNA levels correlate with virus infectivity in clinical samples, Israel, 2022. *Euro Surveill* 2022;27(35):2200636. <http://dx.doi.org/10.2807/1560-7917.ES.2022.27.35.2200636>.

Methods and Applications

Epidemic Surveillance of Influenza Infections: A Network-Free Strategy — Hong Kong Special Administrative Region, China, 2008–2011

Zhanwei Du^{1,✉}; Qi Tan^{2,✉}; Yuan Bai^{1,2}; Lin Wang³; Benjamin J. Cowling^{1,2}; Petter Holme^{4,✉}

ABSTRACT

Introduction: The ease of coronavirus disease 2019 (COVID-19) non-pharmacological interventions and the increased susceptibility during the past COVID-19 pandemic could be a precursor for the resurgence of influenza, potentially leading to a severe outbreak in the winter of 2022 and future seasons. The recent increased availability of data on Electronic Health Records (EHR) in public health systems, offers new opportunities to monitor individuals to mitigate outbreaks.

Methods: We introduced a new methodology to rank individuals for surveillance in temporal networks, which was more practical than the static networks. By targeting previously infected nodes, this method used readily available EHR data instead of the contact-network structure.

Results: We validated this method qualitatively in a real-world cohort study and evaluated our approach quantitatively by comparing it to other surveillance methods on three temporal and empirical networks. We found that, despite not explicitly exploiting the contacts' network structure, it remained the best or close to the best strategy. We related the performance of the method to the public health goals, the reproduction number of the disease, and the underlying temporal-network structure (e.g., burstiness).

Discussion: The proposed strategy of using historical records for sentinel surveillance selection can be taken as a practical and robust alternative without the knowledge of individual contact behaviors for public health policymakers.

Influenza infections were reported to be low between the months of September 2021 and January 2022 (1). The relaxation of coronavirus disease 2019

(COVID-19) non-pharmacological interventions and the increased susceptibility during the past COVID-19 pandemic have provided an opportunity for an increase of more severe influenza epidemics to occur in upcoming winters in temperate locations.

Infectious disease surveillance systems would provide historical information on the occurrence of infections and allow early detection of influenza outbreaks before they are past the point of being contained. The surveillance strategies that map out individual contact behaviors fall into two general categories — those based on static contact networks and those on temporal contact networks. Due to contact networks being essentially dynamic with temporal-network structures [such as burstiness — individual activities often happen in periods of intense activity (2)], the problem remains somewhat more practical in the context of temporal contact networks.

Retrospective studies have demonstrated that temporal network structures can influence the spreading speed and the outbreak size but also surveillance strategies (3–5). Cowling et al. compared two temporal-network strategies to select sentinels [sampling the recent contact, as the recent strategy, and most frequent contact, as the frequent strategy, with random individuals (2)], as well as two static-network strategies (acquaintance and random), on temporal networks for sentinel surveillance of outbreak detection (3). The two temporal-network strategies both derive earlier signals than static-network strategies for early epidemic detection on networks with strong temporal structures. However, due to physical contact data being difficult to obtain, these strategies are difficult to be applied to practical public health systems.

To detect an early signal for the emerging outbreak using sentinel surveillance, the digital data on Electronic Health Records (EHR) provide a unique chance to test cutting-edge sentinel surveillance strategies. The EHR of influenza viruses can help detect other viruses, and have temporal characteristics with records of when individuals were infected. Our previous study found treatment records can be used to

monitor emerging epidemic outbreaks (e.g., influenza) and proposed a simple EHR-based strategy that identifies the most vulnerable individuals who acquired the earliest infections during historical influenza seasons and could be a theoretically optimal surveillance subset (6). However, it does not account for the real-world data validation, the temporal contact networks (in which the contact structure may not be persistent enough), and the cross-strain immunity (which could be gained during an influenza season to protect the previously infected individuals from the reinfection of a group of strains).

In the current study, we produced a practical data-driven surveillance strategy by targeting previously infected nodes with low cross-strain immunity to accelerate outbreak detection using sentinel surveillance of previous earliest infected individuals. We validated this strategy with a real-world cohort study and further validated it by simulations using mathematical epidemic models in temporal networks. We quantified the early warning and Peak lag gained by these selected individuals over different transmission scenarios of effective reproduction numbers, R_{eff} .

METHODS

Cohort Data

In the published dataset (7), serum specimens were collected from a cohort of participants from 2008 to 2011, with each annual record for 956 individuals. We identified an individual to be infected or not using a 4-fold criterion of hemagglutination inhibition (HAI) titers for each study year. Informed by the infection history, we could evaluate the infection probability of a case infected in a year based on the historical records, together with its 95% confidence interval, using the method of one-sample t-test.

Surveillance Strategies

We investigated three temporal-network strategies for designing network-based surveillance systems. To test the generality of our methodology, we compared it with available temporal-network surveillance strategies shown in Cowling et al. using three classes of temporal complex networks with distinct temporal features (Supplementary Material, available in <http://weekly.chinacdc.cn/>) (3).

Epidemic Model

We simulated epidemic outbreaks using a stochastic

chain-binomial model in contact networks with nodes as individuals and edges as epidemiologically relevant contacts between individuals. We used the following two criteria to evaluate the performance of each surveillance strategy in the test epidemic season: Early warning, and Peak lag (Supplementary Material).

Proposed Surveillance Based on Individual Historical Vulnerability

In the static-network study, nodes with higher eigenvector centrality were the theoretical optimal surveillance subset (8). Conversely, nodes, which were infected earlier, tended to have a higher eigenvector centrality (6). We proposed a novel surveillance strategy to target previously infected nodes (History) based on estimating the vulnerability of each individual using their infection history of seasonal respiratory disease (e.g., influenza) registered in the EHR (Figure 1). Let τ_j^i the time at which an individual j acquires infection in season i . We defined the vulnerability of an individual j to contract a respiratory disease by their infection times in influenza season one year ago. This vector ranked each individual in the population by its historical vulnerability to getting infected, which we used as a surveillance strategy.

To be convenient to use by policymakers (e.g., doctors in hospitals), Figure 2 provides a schematic overview of the proposed surveillance strategy with four guidelines. Individuals who were uninfected in the current season but infected in the last season had higher rankings than others, which could have been higher if they had been infected earlier in the last season and had had more infection records in previous seasons.

RESULTS

Real-world Evaluation Using Historical Influenza Infections from a Cohort Study

Informed by a cohort of around 1,000 participants from 2008 to 2011, when influenza A(H1N1)pdm09 circulated, with an annual electronic record of influenza HAI titers (7), we identified an individual to be infected or not using a 4-fold criterion of HAI titers for each study year and estimated the infection probability of a case infected in the third year with/without infection during the past two years (Figure 1A and Supplementary Table S1, available in <http://weekly.chinacdc.cn/>). The participants, who were

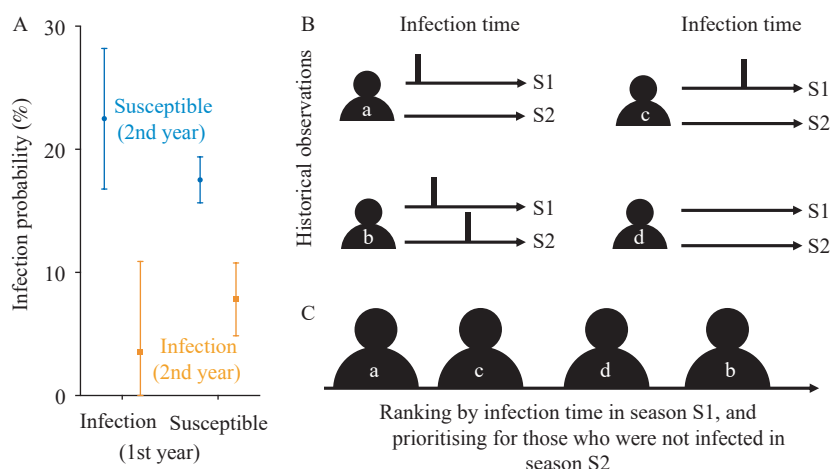


FIGURE 1. A schematic of the proposed surveillance strategy to target previously infected nodes (History). (A) Infection probability of influenza virus in Hong Kong Special Administrative Region. (B) Informed by available historical observations of individuals (a, b, c, and d) over two seasons from S1 to S2, each for one year. (C) In our proposed surveillance strategy, individuals are ranked by the infection time in season S1 for season S2.

Note: In panel A, we studied a cohort of 956 participants from 2008 to 2011 with annual electronic records for three years (2008 to 2010, and 2009 to 2011) (7). We estimated the probability of a case being infected in the third year, which was infected or not in the past two years (Supplementary Table S1, available in <http://weekly.chinacdc.cn/>). Vertical bars and error bars represent the estimated mean and 95% CIs. In panel B, the average historical vulnerability of an individual is estimated from the historical infection time. In panel C, the black bars denote the observed infection timing of individuals in the first and second/third historical seasons.

Abbreviation: S1=the first season; S2=the second season.

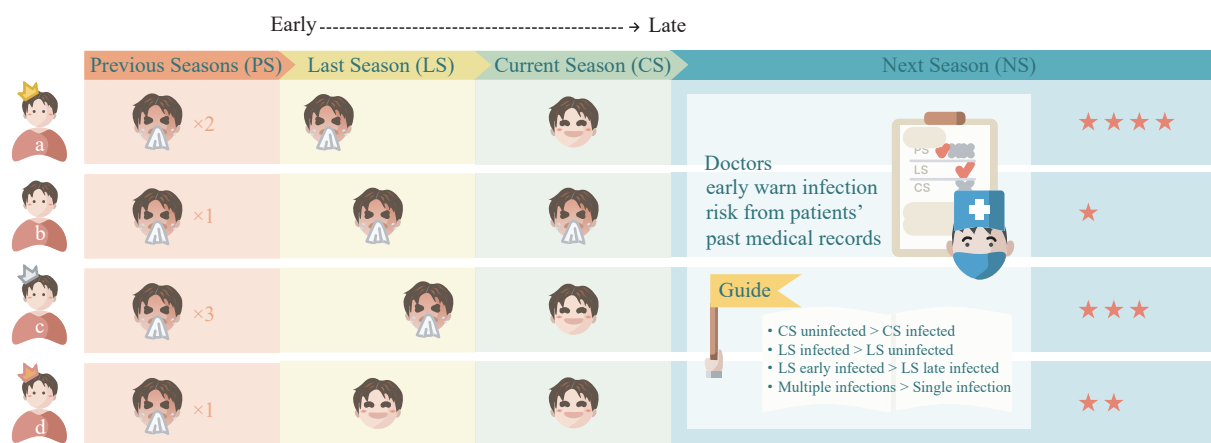


FIGURE 2. A simplified schematic illustration of the proposed surveillance strategy.

Note: The proposed strategy ranks the included individuals following four guidelines. Individuals who were uninfected in the current season but infected in the last season have higher rankings than others. And individuals can get a higher ranking if they were infected earlier in the last season and have more infection records in previous seasons. By taking four individuals (a, b, c, and d) as an example, users (e.g., doctors in hospitals) can assess their electronic records of historical seasons at the end of the current season. Individuals a and c have one infection record in the last season, none in the current season, and are ranked the highest. Given that a has been infected earlier than c, a has a higher ranking than c. If a and c have the same infection times in the last season, we could compare the number of infection records in previous seasons. Finally, the ranking of the four individuals is a, c, d, and b. We used golden/silver/copper crowns and red stars to mark their ranking from high to low.

infected in the first year but not in the second year, had the highest infection probability of 22.49% [95% confidence interval (CI): 16.78%, 28.20%] in the third year (Figure 1A). In the contact network structure,

those participants may have more contact behaviors and low cross-strain immunity in the third year and thus have a higher probability of infection. And historical EHR data can help identify those with higher

infection risks of influenza outbreaks to some extent.

Simulation Evaluation of Surveillance Strategies

We compared our proposed strategy (History) (Figure 1) with three conventional temporal-network-based surveillance strategies, including 1) the recent strategy; 2) the frequent strategy, which uses the top 10% of individuals with the highest numbers of most recent and frequent connections, respectively; and 3) the random acquaintance strategy, which first randomly selects 10% of a randomly selected individual as the surveillance node (Figure 3).

In temporal networks, different from static networks, the experience period for strategy learning may not correlate with the evaluation period for testing, and individual interactions may happen in a short period. This may fail surveillance strategies if the high centrality nodes in the experience period decrease their centrality significantly or interactions in the evaluation period. Thus, we investigate the impact of burstiness [the phenomenon that human activities often happen in intense periods separated by periods of inactivity (2)] and persistence [measured by the fraction of edges that is present both in the first and last 5% of the contacts by the Jaccard similarity coefficient (2)] on the performance of early warning and Peak lags (Supplementary Table S2, available in <http://weekly.chinacdc.cn>). We collected and summarized the properties of the study temporal networks in Supplementary Table S2, with burstiness ranging from 0.39 to 0.72 and persistence ranging from 0 to 0.18.

Burstiness may correlate with the early warning negatively (Supplementary Table S3, available in <http://weekly.chinacdc.cn/>). In the evaluation criteria for early warning, the proposed strategy outstrips the random strategy in all three networks. The performance of our strategy is also comparable to the frequent and recent strategies in the Prostitution and Email networks, but not in the Dating network (which has the highest burstiness) (Figure 4 and Supplementary Table S3). For example, in the Prostitution network, under a low transmission scenario ($R_e=1.2$) and a high transmission scenario ($R_e=3$), the history strategy has an early warning of 1.78 days (95% CI: 0.00, 3.56) and 0.71 days (95% CI: -0.54, 1.95), respectively, which is around a half day earlier than the recent and frequent strategies. In the Dating network, the history strategy is better than

the random strategy but not the other two. As for Peak lag, there is no significant difference among study strategies in the three temporal networks, given the large 95% CI (Figure 4 and Supplementary Table S4, available in <http://weekly.chinacdc.cn>).

DISCUSSION

Although influenza outbreaks are extremely challenging to predict (9), alerting the onset of an influenza pandemic would be extremely important for public health agencies to respond before it pasts the point of being contained.

Building on the availability of electronic health record systems, we proposed a novel surveillance strategy of selecting previously infected individuals for sentinel surveillance in temporal networks. The beauty of this approach is to exploit contact structure without having to measure it — which is both difficult and may change over time, inspired by that history of infection will reflect temporal contact structure if it is persistent enough. In practical use, for a new emerging or reemerging infectious disease, it is not necessary for our proposed strategy to ask for patient infection history or prior knowledge of the same disease.

The proposed strategy does not work well in the Dating network, perhaps due to its high bursty coefficient (Supplementary Table S2). Individuals just have intensive contact for a short period and hinder the subsequent infections. For instance, one individual who has intensive contacts in the training seasons has a higher probability of getting infected than other individuals, and thereby is ranked higher in our proposed history strategy. However, this individual may make few contacts in the test season and has a lower probability to be infected and fail the history strategy.

EHRs are the most essential component of health information technology, with hospital adoption rates representing a country's level of medical digitalization. In China, it was 83.6% and 86.6% in 2018 in China's economically underdeveloped and developed hospitals, respectively (10). Although the growth rate of EHR adoption has been slow since 2013, as a result of many hospitals in underdeveloped areas lacking sufficient financial support and staffing funds, the Chinese government has begun to reform relevant policies, implementing both financial assistance and policy-guiding measures gradually (10). With the implementation of EHR systems in underdeveloped

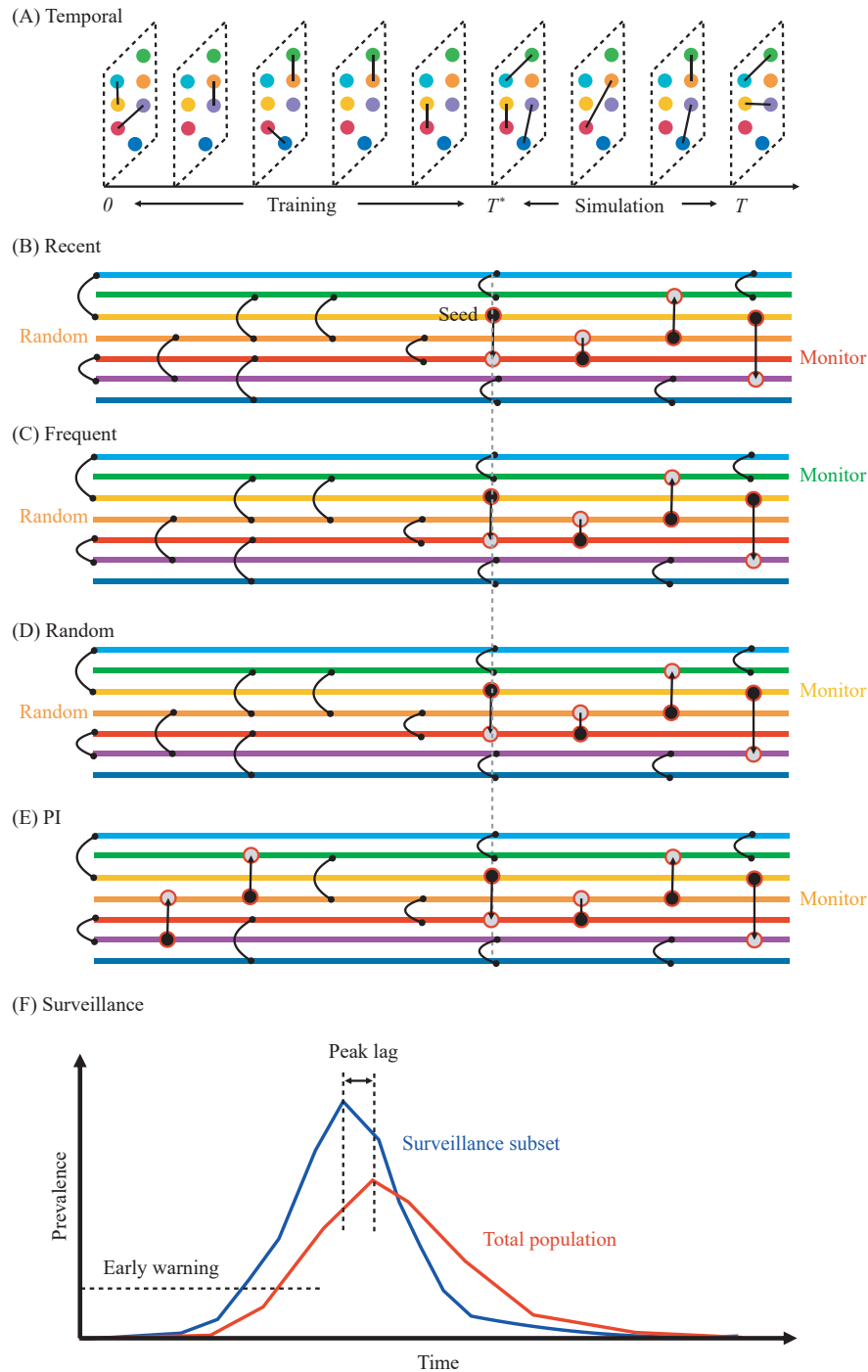


FIGURE 3. Schematic illustration of surveillance strategies. (A) The example of a temporal network with two time phases. (B) The schematic illustration of the Recent surveillance strategy. (C) The schematic illustration of the Frequent surveillance strategy. (D) The schematic illustration of the Random surveillance strategy. (E) The schematic illustration of the history surveillance strategy for previously infected (PI). (F) Surveillance objectives.

Note: In panel A, the first time phase is for training and the second one is for epidemic simulation. In panel B, C, D, and E, the horizontal line denotes an individual and the circles and vertical lines indicate the interaction. We marked the first infected node as “Seed” in the second time window, the node selected randomly to trigger surveillance strategy as “Random”, the node for sentinel surveillance as “Monitor” following different strategies. In epidemic simulation, gray and black circles with red borders denote infectors and infectees, respectively. In panel F, we compared the prevalences between nodes in the surveillance subset and those in the whole population. We calculated the time lag between the two groups reaching 1% prevalence (early warning) and their epidemic peaks (peak lag).

* means the end time of the training phase.

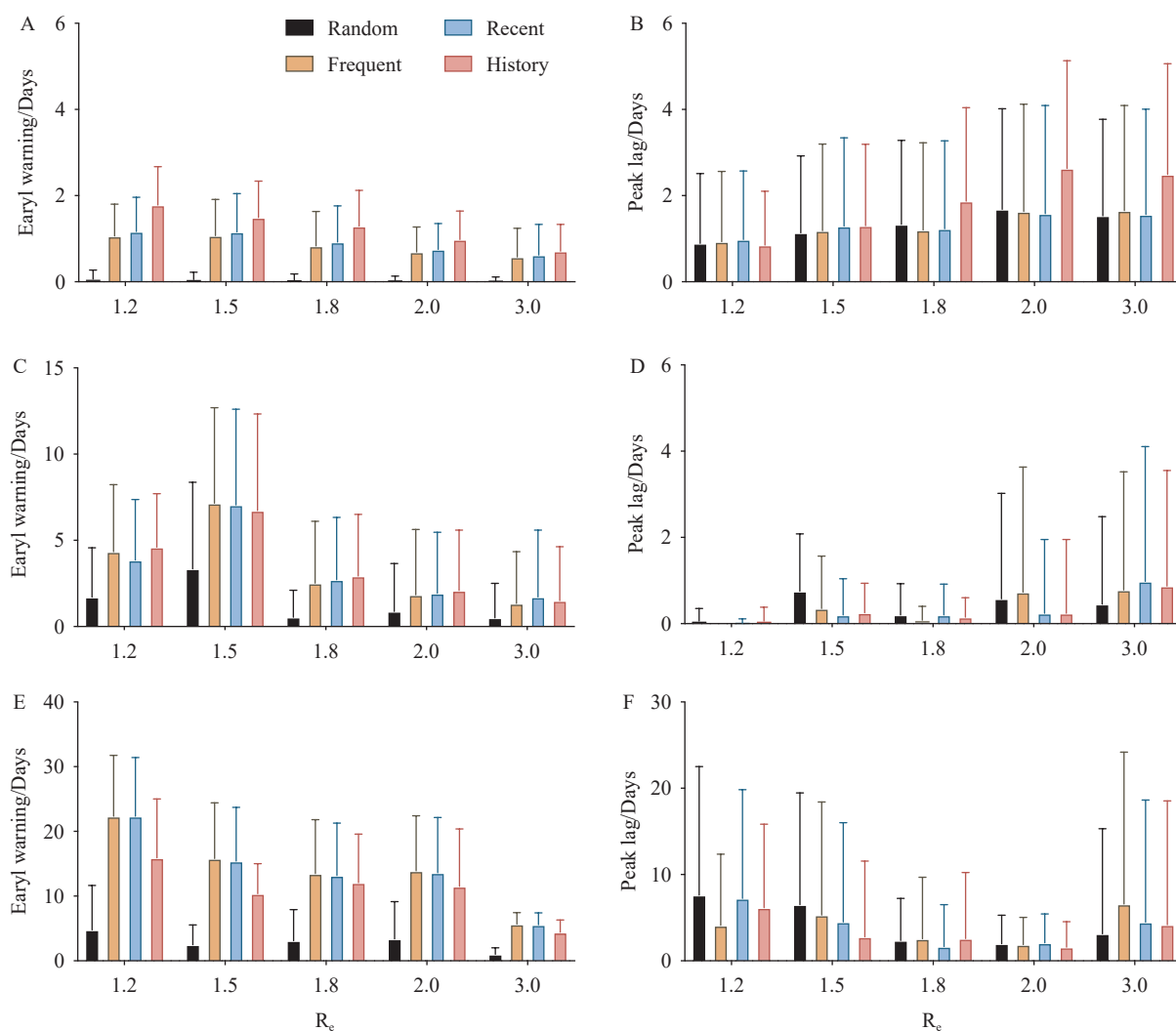


FIGURE 4. Early warning and Peak lag of the random, recent, frequent, and history strategies. (A) Early warning in the Prostitution network. (B) Peak lag in the Prostitution network. (C) Early warning in the Email network. (D) Peak lag in the Email network. (E) Early warning in the Dating network. (F) Peak lag in the Dating network.

Note: The history strategy here uses the EHR records obtained from historical seasons two years ago. The horizontal and vertical axes present the early warning (days) in the left panels and Peak lags (days) in the right panels for each strategy over effective reproduction numbers (R_e). Bars and error bars indicate the mean and standard deviations across 100 simulations of each temporal network. The burstiness of Prostitution, Email, and Dating are 0.39, 0.62, 0.72 (Supplementary Table S2, available in <http://weekly.chinacdc.cn>).

Abbreviation: EHR=Electronic Health Record.

and developed areas in near future, we expect our EHR-based strategy to become increasingly widely used in China.

We concluded that the proposed strategy of using historical records for sentinel surveillance selection is competitive with other existing surveillance strategies in temporal networks and can be taken as a practical and robust alternative without the knowledge of individual contact behaviors for public health policymakers. This study can deepen the understanding of sentinel surveillance and guide future strategies with diverse data sources, especially digital

health data.

Conflicts of interest: BJC consults for AstraZeneca, Fosun Pharma, GlaxoSmithKline, Moderna, Pfizer, Roche and Sanofi Pasteur. BJC is supported by the AIR@innoHK program of the Innovation and Technology Commission of the Hong Kong SAR Government. No other conflicts of interest.

Funding: Supported by Key Projects of Intergovernmental International Scientific and Technological Innovation Cooperation of National Key R&D Programs (No. 2022YFE0112300) and AIR@InnoHK administered by Innovation and

Technology Commission of the Research Grants Council of the Hong Kong SAR Government.

doi: 10.46234/ccdcw2022.207

Corresponding author: Petter Holme, petter.holme@aalto.fi.

¹ WHO Collaborating Centre for Infectious Disease Epidemiology and Control, School of Public Health, Li Ka Shing Faculty of Medicine, The University of Hong Kong, Hong Kong SAR, China; ² Laboratory of Data Discovery for Health Limited (D24H), Hong Kong Science and Technology Park, Hong Kong SAR, China; ³ Department of Genetics, University of Cambridge, Cambridge, UK; ⁴ Department of Computer Science, Aalto University, Espoo, Finland.

[✉] Joint first authors.

Submitted: November 11, 2022; Accepted: November 14, 2022

REFERENCES

1. World Health Organization. Recommended composition of influenza virus vaccines for use in the 2022–2023 northern hemisphere influenza season. 2022. <https://www.who.int/publications/m/item/recommended-composition-of-influenza-virus-vaccines-for-use-in-the-2022-2023-northern-hemisphere-influenza-season>. [2022-10-15].
2. Lee S, Rocha LEC, Liljeros F, Holme P. Exploiting temporal network structures of human interaction to effectively immunize populations. *PLoS One* 2012;7(5):e36439. <http://dx.doi.org/10.1371/journal.pone.0036439>.
3. Bai Y, Yang B, Lin LJ, Herrera JL, Du ZW, Holme P. Optimizing sentinel surveillance in temporal network epidemiology. *Sci Rep* 2017;7(1):4804. <http://dx.doi.org/10.1038/s41598-017-03868-6>.
4. Lloyd-Smith JO, Schreiber SJ, Kopp PE, Getz WM. Superspreading and the effect of individual variation on disease emergence. *Nature* 2005;438(7066):355–9. <http://dx.doi.org/10.1038/nature04153>.
5. Gao C, Zhu JY, Zhang F, Wang Z, Li XL. A novel representation learning for dynamic graphs based on graph convolutional networks. *IEEE Trans Cybern* 2022. <http://dx.doi.org/10.1109/TCYB.2022.3159661>.
6. Du ZW, Bai Y, Wang L, Herrera-Diestra JL, Yuan ZL, Guo RZ, et al. Optimizing COVID-19 surveillance using historical electronic health records of influenza infections. *PNAS Nexus* 2022;1(2):pgac038. <http://dx.doi.org/10.1093/pnasnexus/pgac038>.
7. Tsang TK, Perera RAPM, Fang VJ, Wong JY, Shiu EY, So HC, et al. Reconstructing antibody dynamics to estimate the risk of influenza virus infection. *Nat Commun* 2022;13(1):1557. <http://dx.doi.org/10.1038/s41467-022-29310-8>.
8. Herrera JL, Srinivasan R, Brownstein JS, Galvani AP, Meyers LA. Disease surveillance on complex social networks. *PLoS Comput Biol* 2016;12(7):e1004928. <http://dx.doi.org/10.1371/journal.pcbi.1004928>.
9. World Health Organization. Influenza: are we ready? World Health Organization. <https://www.who.int/news-room/spotlight/influenza-are-we-ready>. [2022-10-15].
10. Liang J, Li Y, Zhang ZA, Shen DX, Xu J, Zheng X, et al. Adoption of Electronic Health Records (EHRs) in China during the past 10 years: consecutive survey data analysis and comparison of Sino-American challenges and experiences. *J Med Internet Res* 2021;23(2):e24813. <http://dx.doi.org/10.2196/24813>.

SUPPLEMENTARY MATERIAL

Methods

Surveillance strategies: We investigated three temporal-network strategies for designing network-based surveillance systems. In a temporal network, we divide the time duration of individual contacts into two sequential periods: the experience period and the evaluation period. The reference strategies used for surveillance are:

- **Random:** target an individual randomly;
- **Recent:** target the most recent contact individual of random individuals in the experience period;
- **Frequent:** target the most frequent contact individual of random individuals in the experience period.

Contact network data sets: To test the generality of our methodology, we also compared it with available temporal-network surveillance strategies shown in Bai et al. (1), using three classes of temporal complex networks with distinct temporal features:

● **Prostitution:** A sexual network, collected from a Brazilian online forum, includes N=16,730 individuals and E=50,632 sexual contacts over T=2,232 days. The contact at a given time represents the reported sexual encounter between a male sex buyer and a female escort (2–3).

● **Email:** A communication network, collected from one of the main mail servers of a university (4), includes N=2,997 email accounts and E=202,694 contacts over T=82 days. The contact at time t represents the interaction of two email accounts by sending or receiving a message (2,4).

● **Dating:** A sexual network, collected from an Internet dating community (5), includes N=28,972 individuals as well as E=430,827 sexual contacts over a span of T=512 days. Each contact demonstrates the initial dating interaction between two individuals (2,5).

The degree distributions of all three temporal networks follow a power law (1). Additionally, they show different degrees of burstiness (the phenomenon that human activities often happen intensively in short periods separated by periods of quiescence (2)) and persistence [the fraction of edges that is present both in the first and last 5% of the contacts by the Jaccard similarity coefficient (2)].

The three temporal networks show high values of burstiness with Prostitution at 0.39, Dating at 0.62, and Email at 0.72. At the same time, they possess different values of persistence, with Prostitution and Dating as 0, and Email as 0.18 (1).

The time scales of the temporal contacts in the above three datasets are greatly different. The mean number of contacts per individual in 7 days in prostitution, email, and dating datasets are 0.8, 18.4, and 16.1, respectively. We rescaled the time scales of the temporal contacts in these datasets to reduce the difference in physical contacts that

SUPPLEMENTARY TABLE S1. Infection probability of influenza virus in Hong Kong Special Administrative Region.

Infected in first year	Infected in second year	Mean infection probability in third year	Number of cases
Yes	No	22.49% (95% CI: 16.78%, 28.20%)	209
No		17.53% (95% CI: 15.66%, 19.39%)	1,592
Yes	Yes	3.57% (95% CI: 0.00%, 10.90%)	28
No		7.81% (95% CI: 4.86%, 10.77%)	320

Note: We estimated from a cohort of 956 participants from 2008 to 2011 with annual electronic records (1). We separated the four-year dataset into two three-year sub-datasets of 2008 to 2010 and 2009 to 2011. Cases were selected following different criteria from the two sub-datasets and aggregated together to estimate the infection probability in the third year. We estimated the probability of a case infected in the third year, which was infected or not in the past two years.

Abbreviation: CI=confidence interval.

SUPPLEMENTARY TABLE S2. Properties of temporal networks.

Dataset	Number of nodes	Number of edges	Time steps	Time unites	Average degree	Burstiness	Persistence
Prostitution	16,730	50,632	2,232 days	1 day	15	0.39	0
Email	2,997	202,694	82 days	1 second	15	0.62	0.18
Dating	28,972	430,827	512 days	1 second	8	0.72	0

SUPPLEMENTARY TABLE S3. Early warning (days) of optimal testing strategies for various influenza transmission scenarios.

<i>R</i>	Network	Random Mean (95% CI)	Frequent Mean (95% CI)	Recent Mean (95% CI)	History Mean (95% CI)
1.2	Prostitution	0.06 (−0.35, 0.47)	1.06 (−0.43, 2.54)	1.17 (−0.41, 2.75)	1.78 (0.00, 3.56)
1.5		0.05 (−0.28, 0.39)	1.07 (−0.61, 2.76)	1.16 (−0.61, 2.94)	1.49 (−0.21, 3.18)
1.8		0.04 (−0.24, 0.33)	0.83 (−0.77, 2.42)	0.92 (−0.77, 2.61)	1.29 (−0.37, 2.94)
2		0.03 (−0.17, 0.24)	0.69 (−0.47, 1.85)	0.75 (−0.45, 1.95)	0.98 (−0.35, 2.31)
3		0.02 (−0.16, 0.21)	0.58 (−0.73, 1.89)	0.62 (−0.79, 2.04)	0.71 (−0.54, 1.95)
1.2	Email	1.71 (−4.01, 7.43)	4.35 (−3.40, 12.11)	3.86 (−3.15, 10.87)	4.60 (−1.58, 10.77)
1.5		3.34 (−6.71, 13.40)	7.15 (−3.96, 18.26)	7.05 (−4.08, 18.18)	6.72 (−4.47, 17.91)
1.8		0.54 (−2.60, 3.68)	2.52 (−4.66, 9.69)	2.72 (−4.50, 9.95)	2.92 (−4.22, 10.05)
2		0.88 (−4.65, 6.42)	1.84 (−5.74, 9.41)	1.93 (−5.14, 9.00)	2.08 (−4.91, 9.07)
3		0.51 (−3.47, 4.50)	1.34 (−4.68, 7.35)	1.72 (−6.04, 9.48)	1.49 (−4.77, 7.74)
1.2	Dating	4.79 (−8.91, 18.49)	22.35 (3.52, 41.17)	22.35 (4.21, 40.49)	15.91 (−2.26, 34.08)
1.5		2.48 (−3.68, 8.65)	15.81 (−1.39, 33.01)	15.42 (−1.15, 31.99)	10.39 (1.14, 19.64)
1.8		3.10 (−6.52, 12.72)	13.49 (−3.14, 30.12)	13.17 (−3.05, 29.40)	12.07 (−2.96, 27.11)
2		3.38 (−8.14, 14.89)	13.90 (−3.17, 30.97)	13.60 (−3.51, 30.70)	11.52 (−6.18, 29.22)
3		1.01 (−1.01, 3.03)	5.69 (2.18, 9.21)	5.59 (1.98, 9.21)	4.43 (0.64, 8.22)

Abbreviation: CI=confidence interval.

SUPPLEMENTARY TABLE S4. Peak time (days) of optimal testing strategies for a range of influenza transmission scenarios.

<i>R</i>	Network	Random Mean (95% CI)	Frequent Mean (95% CI)	Recent Mean (95% CI)	History Mean (95% CI)
1.2	Prostitution	0.89 (−2.35, 4.12)	0.93 (−2.32, 4.18)	0.98 (−2.19, 4.16)	0.85 (−1.66, 3.35)
1.5		1.14 (−2.42, 4.70)	1.19 (−2.84, 5.22)	1.29 (−2.81, 5.38)	1.30 (−2.48, 5.08)
1.8		1.33 (−2.57, 5.22)	1.20 (−2.86, 5.26)	1.23 (−2.84, 5.31)	1.87 (−2.47, 6.21)
2		1.68 (−3.00, 6.36)	1.63 (−3.35, 6.61)	1.58 (−3.45, 6.61)	2.63 (−2.37, 7.62)
3		1.53 (−2.96, 6.02)	1.65 (−3.22, 6.52)	1.56 (−3.34, 6.46)	2.49 (−2.65, 7.62)
1.2	Email	0.06 (−0.53, 0.65)	0.00 (0.00, 0.00)	0.01 (−0.18, 0.20)	0.06 (−0.58, 0.69)
1.5		0.75 (−1.92, 3.42)	0.35 (−2.10, 2.79)	0.20 (−1.48, 1.89)	0.25 (−1.14, 1.64)
1.8		0.20 (−1.26, 1.65)	0.08 (−0.55, 0.72)	0.20 (−1.25, 1.64)	0.15 (−0.74, 1.04)
2		0.58 (−4.31, 5.46)	0.73 (−5.07, 6.53)	0.24 (−3.18, 3.66)	0.24 (−3.18, 3.66)
3		0.45 (−3.61, 4.51)	0.78 (−4.70, 6.26)	0.98 (−5.27, 7.24)	0.87 (−4.49, 6.22)
1.2	Dating	7.61 (−22.17, 37.38)	4.12 (−12.37, 20.60)	7.23 (−17.98, 32.43)	6.17 (−13.17, 25.50)
1.5		6.50 (−19.41, 32.41)	5.31 (−20.90, 31.53)	4.51 (−18.49, 27.52)	2.78 (−14.79, 20.34)
1.8		2.37 (−7.37, 12.11)	2.56 (−11.69, 16.80)	1.67 (−8.00, 11.34)	2.58 (−12.72, 17.87)
2		1.99 (−4.61, 8.59)	1.90 (−4.39, 8.18)	2.09 (−4.59, 8.76)	1.58 (−4.33, 7.49)
3		3.15 (−21.15, 27.45)	6.60 (−28.58, 41.79)	4.48 (−23.82, 32.78)	4.18 (−24.55, 32.90)

Abbreviation: CI=confidence interval.

the infectious virus transmits on (6). Specifically, we sped up the time scale of the prostitution dataset 40-fold and slowed down the time scales of the email and dating by mapping the one-day time scale in the email dataset and the two-day time scale in the dating dataset to seven-day, respectively. Finally, the mean estimates are closer among prostitution, email, and dating datasets, which are 2.97, 3.97, and 9.06 days on average in 7 days.

SUPPLEMENTARY TABLE S5. Values of parameters in the SIRS epidemic model in networks across effective reproduction numbers.

Network	Effective reproduction number R_e	Transmission probability β	Recover rate γ (days)
Prostitution	1.2	0.3	7
	1.5	0.4	7
	1.8	0.5	7
	2	0.7	7
	3	0.9	7
Email	1.2	0.15	7
	1.5	0.3	7
	1.8	0.5	7
	2	0.6	7
	3	0.8	7
Dating	1.2	0.2	7
	1.5	0.3	7
	1.8	0.35	7
	2	0.4	7
	3	0.8	7

Abbreviation: SIRS=susceptible-infectious-recovered-susceptible.

Epidemic Model

We simulated epidemic outbreaks using a stochastic chain-binomial model in contact networks with nodes as individuals and edges as epidemiologically relevant contacts between individuals.

We simulated the susceptible-infectious-recovered-susceptible (SIRS) model: each individual has three states: susceptible (S), infectious (I), or recovered (R). The transmission probability of the disease in each contact is β . The node i will remain infectious for $1/\gamma$ days, after which it will recover. For each dataset, we simulate multiple instances of β and γ . We set γ to 7 days as the base recovery period (7). The γ is calibrated to match the expected R_e . The values of β and γ used in the experiments are listed in Supplementary Table S5. We estimated R_e by the secondary infections of the earliest infected cases, which count for 1% of the population. We started simulations in temporal networks by randomly sampling one seed to be infectious.

The disease prevalence is counted as the number of infectious people over time. We divided the temporal contacts into $\eta=4$ phases, with each phase as one season. In each phase, we randomly selected one individual as the source of infection. To simulate the cross-immunity, we asserted that the individual infected in the previous season will not be infected in the current season, as that the immunity period of influenza had been over one year (8–9). We used the last season as the test epidemic season and used the contact information data in the previous $\eta-1$ seasons for training surveillance strategies.

Following (10–12), we used the following two criteria to evaluate the performance of each surveillance strategy in the test epidemic season:

- Early warning. Let t_μ^{EP} be the time at which the disease prevalence reaches a predefined threshold μ in the entire population (EP), and t_μ^{SG} the time at which the disease prevalence reaches the same threshold $\mu=1\%$ in the surveillance group (SG). The early warning criterion measures the time lag $t_\mu^{EP} - t_\mu^{SG}$.

- Peak lag. Let t_{peak}^{EP} , t_{peak}^{SG} be the time at which the disease prevalence reaches the peak prevalence in the entire population and in the surveillance group, respectively. Peak lag criterion measures the time lag $t_{peak}^{EP} - t_{peak}^{SG}$.

Limitations

We would highlight several limitations in our study. First, we assumed the consequent outbreaks have similar circulating strains over seasons in our simulations, and individuals infected last season have immunity protection against infection in the consequent season. However, if the circulating strains are different during two consecutive

influenza seasons, there is weak cross-immunity protection. In this situation, the previously infected individuals in the last outbreak may be chosen directly for the sentinel surveillance of the studied outbreak. Second, the lack of influenza circulation in the past seasons during 2020 and 2021 would reduce the immunity level in the population level (13). For the sentinel surveillance of outbreaks in the winter of 2022, we suggest the selection of individuals based on EHR data before the COVID-19 pandemic, for example, in the winter of 2019. Third, we did not model the influenza vaccination in our simulations significantly. However, the effective reproduction number in our simulations has included the impact of vaccinations on transmissions, with higher vaccine coverage resulting in lower effective reproduction numbers. To reduce this potential bias in practice, we suggest excluding those individuals vaccinated in the near period in the sentinel surveillance set. Fourth, it is plausible that not all infected individuals will seek treatment and leave their records. According to our prior study (14), the EHR-based strategy did not work well when the probability of seeking treatment and having an influenza record does not exceed 25%, which we believe also holds in the temporal network qualitatively. Fifth, in the study of temporal networks, we mainly considered the individual contacts. Environmental variables may have an inevitable effect in determining whether a pathogen can become epidemic, for example, absolute humidity and temperature on influenza (15–16). We may include these additional effects on the transmission rate in the future for disease modeling of specific infectious diseases. Sixth, we divided the time duration of temporal networks into the experience and evaluation periods. However, human movements have seasonal patterns (17), which may enhance the performance of our proposed strategy. For the example of winter influenza, we may only use the history of winter influenza for the proposed strategy to learn, but not the overall annual history of influenza infection. Seventh, to validate our assumption of the impact of cross-immunity on early surveillance, we conducted a real-world evaluation using historical influenza infections from a cohort study. Although the group following the EHR-based strategy had a higher relative infection probability than other groups, influenza transmission is complex and has age-specific heterogeneity, which is not included in our modeling. However, we believe our result still holds qualitatively.

REFERENCES

- Bai Y, Yang B, Lin LJ, Herrera JL, Du ZW, Holme P. Optimizing sentinel surveillance in temporal network epidemiology. *Sci Rep* 2017;7(1):4804. <http://dx.doi.org/10.1038/s41598-017-03868-6>.
- Lee S, Rocha LEC, Liljeros F, Holme P. Exploiting temporal network structures of human interaction to effectively immunize populations. *PLoS One* 2012;7(5):e36439. <http://dx.doi.org/10.1371/journal.pone.0036439>.
- Rocha LEC, Liljeros F, Holme P. Information dynamics shape the sexual networks of Internet-mediated prostitution. *Proc Natl Acad Sci USA* 2010;107(13):5706–11. <http://dx.doi.org/10.1073/pnas.0914080107>.
- Eckmann JP, Moses E, Sergi D. Entropy of dialogues creates coherent structures in e-mail traffic. *Proc Natl Acad Sci USA* 2004;101(40):14333–7. <http://dx.doi.org/10.1073/pnas.0405728101>.
- Holme P, Edling CR, Liljeros F. Structure and time evolution of an Internet dating community. *Soc Networks* 2004;26(2):155–74. <http://dx.doi.org/10.1016/j.socnet.2004.01.007>.
- Feehan DM, Mahmud AS. Quantifying population contact patterns in the United States during the COVID-19 pandemic. *Nat Commun* 2021;12(1):893. <http://dx.doi.org/10.1038/s41467-021-20990-2>.
- CDC. Key Facts About Influenza (Flu). Centers for Disease Control and Prevention. 2022. <https://www.cdc.gov/flu/about/keyfacts.htm>. [2022-11-3].
- Patel MM, York IA, Monto AS, Thompson MG, Fry AM. Immune-mediated attenuation of influenza illness after infection: opportunities and challenges. *Lancet Microbe* 2021;2(12):e715–25. [http://dx.doi.org/10.1016/S2666-5247\(21\)00180-4](http://dx.doi.org/10.1016/S2666-5247(21)00180-4).
- Pei S, Teng X, Lewis P, Shaman J. Optimizing respiratory virus surveillance networks using uncertainty propagation. *Nat Commun* 2021;12(1):222. <http://dx.doi.org/10.1038/s41467-020-20399-3>.
- Herrera JL, Srinivasan R, Brownstein JS, Galvani AP, Meyers LA. Disease surveillance on complex social networks. *PLoS Comput Biol* 2016;12(7):e1004928. <http://dx.doi.org/10.1371/journal.pcbi.1004928>.
- Thompson WW, Comanor L, Shay DK. Epidemiology of seasonal influenza: use of surveillance data and statistical models to estimate the burden of disease. *J Infect Dis* 2006;194(S2):S82–91. <http://dx.doi.org/10.1086/507558>.
- Rath TM, Carreras M, Sebastiani P. Automated detection of influenza epidemics with hidden Markov models. In: *Proceedings of the 5th international symposium on intelligent data analysis on advances in intelligent data analysis V*. Berlin: Springer. 2003:521–32. http://dx.doi.org/10.1007/978-3-540-45231-7_48.
- Baker RE, Park SW, Yang WC, Vecchi GA, Metcalf CJE, Grenfell BT. The impact of COVID-19 nonpharmaceutical interventions on the future dynamics of endemic infections. *Proc Natl Acad Sci USA* 2020;117(48):30547–53. <http://dx.doi.org/10.1073/pnas.2013182117>.
- Du ZW, Bai Y, Wang L, Herrera-Diestra JL, Yuan ZL, Guo RZ, et al. Optimizing COVID-19 surveillance using historical electronic health records of influenza infections. *PNAS Nexus* 2022;1(2):pgac038. <http://dx.doi.org/10.1093/pnasnexus/pgac038>.
- Shaman J, Kohn M. Absolute humidity modulates influenza survival, transmission, and seasonality. *Proc Natl Acad Sci USA* 2009;106(9):3243–8. <http://dx.doi.org/10.1073/pnas.0806852106>.
- Deyle ER, Maher MC, Hernandez RD, Basu S, Sugihara G. Global environmental drivers of influenza. *Proc Natl Acad Sci USA* 2016;113(46):13081–6. <http://dx.doi.org/10.1073/pnas.1607747113>.
- Wesolowski A, Zu Erbach-Schoenberg E, Tatem AJ, Lourenço C, Viboud C, Charu V, et al. Multinational patterns of seasonal asymmetry in human movement influence infectious disease dynamics. *Nat Commun* 2017;8(1):2069. <http://dx.doi.org/10.1038/s41467-017-02064-4>.

Methods and Applications

Uncovering the Impact of Control Strategies on the Transmission Pattern of SARS-CoV-2 — Ruili City, Yunnan Province, China, February–March 2022

Jinou Chen¹; Yubing Qiu¹; Yuhua Shi¹; Wei Wu¹; Erda Zheng¹; Lin Xu^{1,†}; Manhong Jia^{1,†}

ABSTRACT

Introduction: The implementation of public health and social measures (PHSMs) was an effective option for controlling coronavirus disease 2019 (COVID-19). However, evidence is needed to evaluate these PHSMs' effects on the recently emerged variant Omicron.

Methods: This study investigated variant Omicron BA.2's outbreak in Ruili City, Yunnan Province, China. The disease transmission dynamics, spatiotemporal interactions, and transmission networks were analyzed to illustrate the effect of PHSM strategies on Omicron spread.

Results: A total of 387 cases were related to the outbreak. The time-varying reproduction number was synchronized with PHSM strategies. Spatiotemporal clustering strength presented heterogeneity and hotspots. Restricted strategies suppressed temporal and spatial relative risk compared with routine and upgraded strategies. The transmission network presented a steeper degree distribution and a heavier tail under upgraded strategies. Phase transformation and distinctive transmission patterns were observed from strategy-stratified subnetworks.

Conclusions: The tightened response strategy contained reproduction of the virus, suppressed spatiotemporal clustering, and reshaped the networks of COVID-19 Omicron variant transmission. As such, PHSMs against Omicron are likely to benefit future responses as well.

INTRODUCTION

The emergence of severe acute respiratory syndrome coronavirus 2 (SARS-CoV-2) led to a global pandemic. Several waves of the pandemic have been associated with different variants of SARS-CoV-2 over the past two years. The most recent variant has been the Omicron variant. This variant raises concern due to its ability to bypass pre-existing immunity acquired

through vaccination: a mutation that has led to increased transmissibility (1–2). Low vaccine efficacy and highly contagious Omicron variant emergence have jointly highlighted existing public health measurements (3). In the absence of effective drugs, the implementation of public health and social measures (PHSMs) is an effective option and the best practical tool for responding to coronavirus disease 2019 (COVID-19) spread. Thus, field evidence and study of PHSMs' impact on the Omicron variant transmission are urgent and essential.

Ruili has been on the front line of fighting against COVID-19; this southwestern city has endured and responded to multiple waves of the pandemic since 2020 (4). Ruili offers a unique opportunity to study the effect of PHSMs on COVID-19 transmission — especially insofar as how it manifests within China. More detailed characteristics about Ruili can be found in the Supplementary Materials (available in <http://weekly.chinacdc.cn/>).

This study investigated the Omicron BA.2 variant outbreak in Ruili to assess different PHSM strategies' impact on transmission dynamics and spatial-temporal interaction. Ultimately, the study was able to illustrate transmission networks based on the different PHSM scenarios — which helps deepen understanding of its impact on COVID-19 prevention and control.

METHODS

Data Source and Collection

This study's data collection was based on field research in Ruili investigating a COVID-19 Omicron BA.2 variant outbreak that occurred between February 14 and March 29, 2022. For each COVID-19 case, the data attributes noted included gender, age, type of case, symptom onset date, exposure date, individual residence address, and whether the case involved a vaccinated person or not. This study then identified close contact relationships and constructed epidemiological links based on a detailed

epidemiological investigation. Finally, it mapped the individual address to the latitudes and longitudes by the Gaode geocoding Application Programming Interface for further analysis.

The PHSMs and Control Strategies

The PHSMs included nucleic acid screening, tracing and management of close contacts, border trade management, in-city travel control, risk site control, outgoing traveler control, personal protection, and social distancing. The various PHSMs were grouped into four comprehensive strategies throughout the outbreak (Figure 1B). Different PHSMs strategies were synchronized to the intensity of the outbreak.

Data Analysis

Statistical analyses were done by using R software (version 4.0.2, R Core Team, Vienna, Austria). The transmission networks were visualized using Gephi software (version 0.9.4, Bastian M, San Jose, California, USA). The statistical significance level was set at $P < 0.05$.

The Transmission Characteristics and Dynamics

The epidemic curve was depicted to illustrate the outbreak. The demographics of cases were also described and grouped based on the PHSM scenarios.

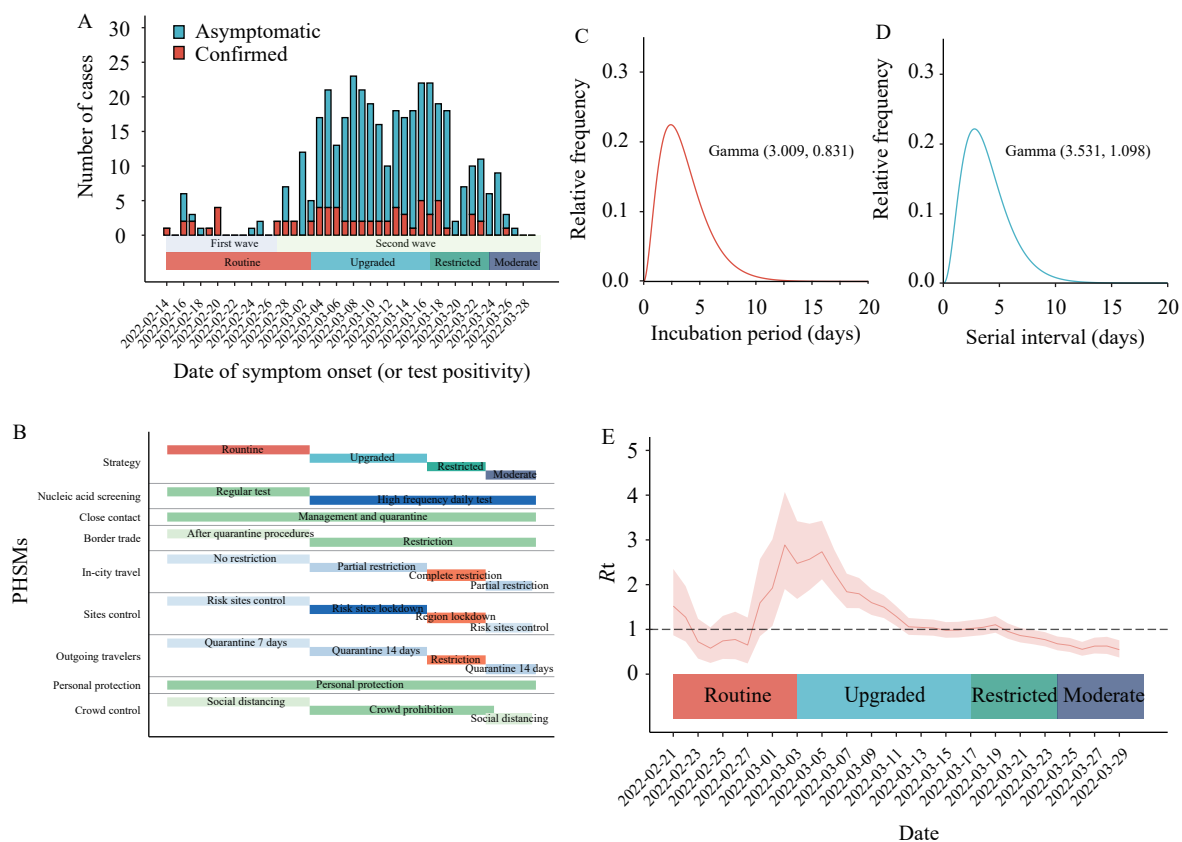


FIGURE 1. The epidemic and transmission dynamics synchronized with PHSM strategies from the COVID-19 outbreak in Ruili, China, February–March 2022. (A) The epidemic curve of COVID-19 outbreak (B) The synchronized PHSM strategies for outbreak control. (C) The estimated parameters and distribution of the incubation period. (D) The estimated parameters and distribution of the serial interval. (E) The R_t and its 95% CrI of COVID-19 transmission under PHSM strategies.

Note: Panel A presents the first wave of outbreak: from February 14 to 26. Thereafter, the second wave from February 27 to March 29. Panel B shows the PHSM implementations and strategies. The routine strategy was implemented between February 14 and March 2, the upgraded strategy between March 3 and 16, the restricted strategy between March 17 and 24, and the moderate strategy between March 25 and 29. Panel C and D estimates the distribution and parameters of the incubation period and the serial interval. Panel E presents the R_t of the outbreak. Based on the previous fitted serial interval distribution and the case incidence time series, the 7-day moving average R_t and its 95% CrI were calculated throughout the outbreak. The R_t being less than 1 indicated transmission was interrupted and contained; otherwise, the transmission was ongoing.

Abbreviation: COVID-19=coronavirus disease 2019; PHSM=public health and social measure; R_t =time-varying reproduction number; 95% CrI=95% credible interval.

This study then fitted four distributions (Normal, Log-normal, Gamma, and Weibull) and estimated distribution parameters for the disease incubation period and serial interval. It determined the best-fitted distributions with the minimal Akaike information criterion. Finally, this study estimated the basic reproduction number (R_0) and the time-varying reproduction number (R_t) in order to evaluate the PHSM strategies' effect on Omicron transmission.

The Spatial-temporal Interaction and Risk Evaluation

This investigation applied the Knox test to quantify the effect of PHSM strategies on the spatial-temporal interaction of viral transmission. A detailed introduction of the Knox test can be found in the Supplementary Materials. In brief, the method defines spatial-temporal interaction as pairs of cases that are close in both spatial distance and temporal interval; thus, it can uncover spatiotemporal hotspots on a defined scale. The test provided spatiotemporal clustering strength (S) and relative risk (RR) calculations based on the comparison of observed (A_X) and expected (E_X) values of the Knox statistic X.

This study further analyzed the S by fitting the overall and strategy-specified mixed linear model (MLM) into spatiotemporal-repeated structural data. The MLM fixed effect of PHSM strategies was estimated to compare its effect on spatiotemporal clustering. The aggregated RR was depicted by spatial and temporal variation to identify spatiotemporal clustering risks under different PHSM strategies.

The Transmission Networks Analysis

To analyze the effect of PHSM strategies on transmission relationships, this study applied transmission network analysis to the data through the construction of transmission networks based on close contact relationships and epidemiological links between cases. Each case was defined as a node, and the connection between two cases was defined as an edge in the network. Through this, the transmission network could then be illustrated as a graphic expression. The PHSM strategies' effect on the transmission pattern was evaluated and compared by overall and strategy-specified network parameters. More details on the network parameters can be found in the Supplementary Materials.

RESULTS

The Characteristics and Dynamics of the Transmission

On February 16, two index cases were identified that shared the same RNA sequence as lineage BA.2 (Omicron variant); another index case was identified as lineage B.1.617.2 (Delta variant). The subsequent cases were all sequenced and identified as Omicron variant BA.2 (no more Delta variant infections appeared). Up until March 29, a total of 387 cases were related to the variant BA.2 outbreak over the course of 43 days (Figure 1A). The characteristics of these cases were summarized in Supplementary Table S1 (available in <http://weekly.chinacdc.cn/>).

The incubation period of measured cases followed a gamma distribution (Figure 1C); the mean incubation period was 3.6 days; and standard deviation (SD) was 2.1 days. The serial interval fitted best with gamma distribution (Figure 1D); the mean serial interval was 3.2 days, and SD was 1.7 days. From February 14 to March 29, the R_0 was 1.1 [95% credible interval (CrI): 1.1 to 1.2]. The R_t varied according to PHSM strategies (Figure 1E); the average R_t under four PHSM strategies were 1.27, 1.65, 0.91, and 0.60, respectively.

The Spatial-temporal Risk Evaluation

The median spatial distance between pairs of cases was 16.3 kilometers. Spatiotemporal clustering strength presented heterogeneity and hotspots (Figure 2A–B). The highest clustering strength $S_{\max}=314.7$ was a time interval from 1 to 2 days and a distance within 100 meters. There was a relatively high clustering strength within 4 days and 1 kilometer. The MLM fixed effects of S were shown in Figure 2C–D. The fixed effects of MLM were 17.89, 1.97, -1.53, and -8.59 for the routine, upgraded, restricted, and moderate strategies respectively. The S decreased steeply with increasing spatial distance ($\beta_s=-0.86$ per 0.1 kilometers), but it presented a prolonged tail while temporal intervals increased ($\beta_t=-1.38$ per day).

The aggregated analysis showed that the restricted strategy suppressed temporal RR between 4 and 7 days in comparison with the routine and upgraded strategies (Figure 2E). The restricted strategy (RR=1.20) reduced 60% and 19% spatial risk compared with the routine (RR=1.80) and upgraded strategies (RR=1.39), while the spatial distance was equal to zero (Figure 2F). The overall RR was significantly different under PHSM strategies (Figure 2G).

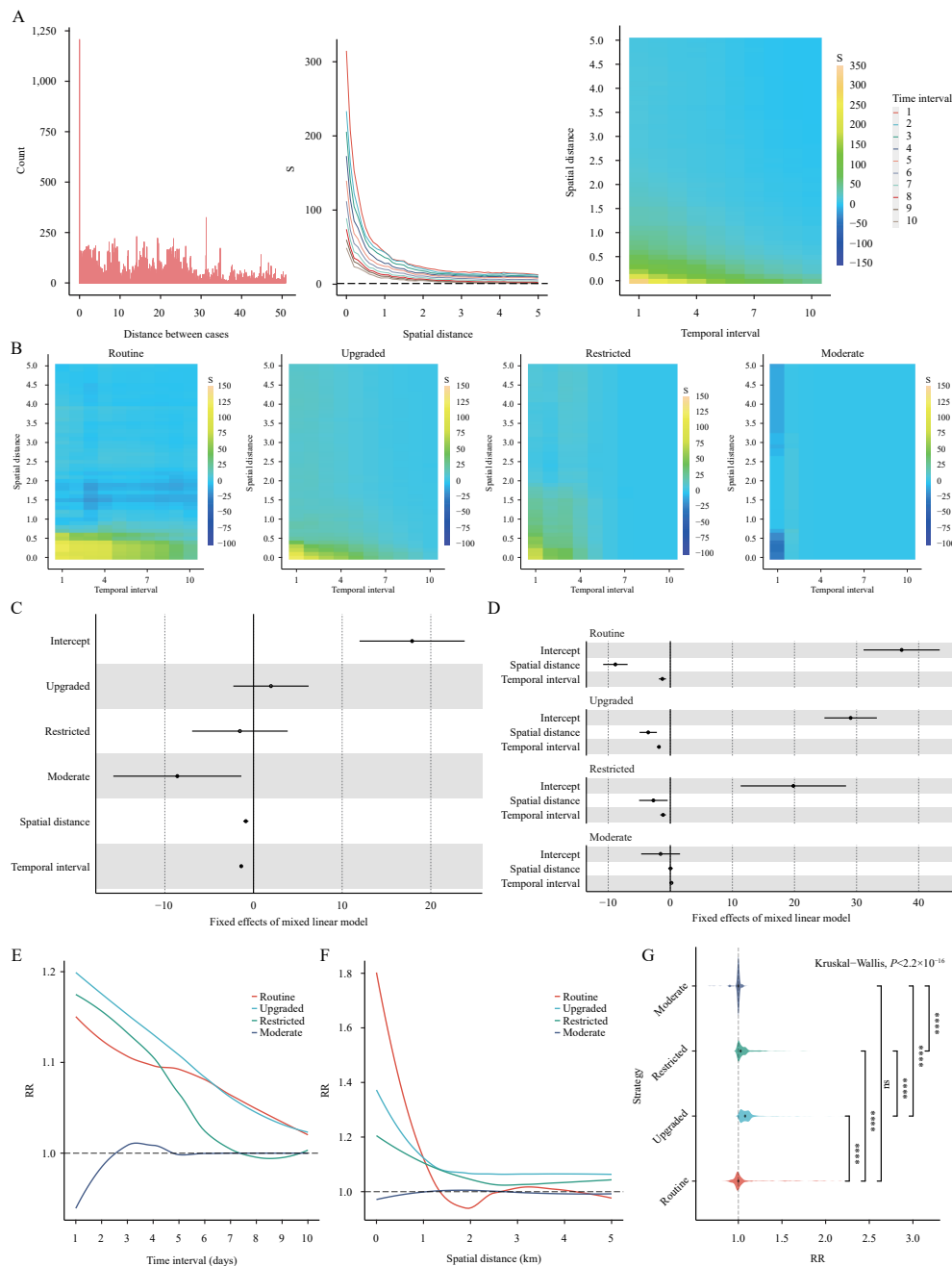


FIGURE 2. The spatial-temporal interaction of the COVID-19 outbreak in Ruili, China, February–March 2022. (A) The spatial distance of COVID-19 incidence and spatial-temporal interaction of the overall strength of transmission. (B) The spatial-temporal interaction of the strategy-stratified strength of transmission. (C) The overall fixed effect of spatiotemporal clustering strength. (D) The strategy-stratified fixed effect of spatiotemporal clustering strength. (E) The characterization of strategy-stratified relative risk in temporal scale. (F) The characterization of strategy-stratified relative risk on a spatial scale. (G) The overall spatiotemporal relative risks of PHSM strategies.

Note: Panel A and Panel B presents the overall and strategy-stratified distance between cases, and the S projected into temporal interval and spatial distance. Panel C and Panel D showed that the S regressed with PHSM strategies spatial distance and temporal interval by applying the MLM. The point and interval presented the mixed linear regression coefficient β_i and its 95% confidence interval; the solid circle was regression coefficient test $P < 0.05$; and, finally, the hollow circle was $P \geq 0.05$. Panel E–G presents the aggregated RR projected to temporal interval and spatial distance, and the multiple comparison of RR under strategies was applied through the nonparametric Bonferroni test.

**** $P < 0.05$; ns: $P \geq 0.05$.

Abbreviation: COVID-19=coronavirus disease 2019; PHSM=public health and social measure; MLM=mixed linear model; S=the clustering strength; RR=the relative risk.

Transmission Network Analysis

As shown in Figure 3, this study constructed a transmission network. The network showed highly connected nodes, indicating dense consociation of transmission. The degree distribution of the upgraded subnetwork was steeper and had a heavier tail than other subnetworks: the long tail of degree distribution means a super-spreader exists.

Phase transformation was observed between subnetworks. The subnetworks under different strategies showed heterogeneity of parameters, scale, and transmission patterns (Table 1). The maximum degree (k_{max}) and average degree (k_{aver}) indicated more serious transmission intensity for the upgraded and restricted subnetworks. The subnetwork pattern for the upgraded strategy displayed an uncontrolled, super-spreader, large-scale, scattered, and widespread

network; it also denoted a larger γ , d , and l_{aver} , as well as a smaller c_{aver} . On the other hand, the subnetwork pattern of the restricted strategy presented a lessened, highly condensed subnetwork with contained scale and suppressed connectivity; it denoted a smaller γ , d , l_{aver} , as well as a larger c_{aver} . The shared pattern across the routine and moderate subnetworks represented similar PHSM strategy implementation and effect.

DISCUSSION

In brief, the evidence collected by this study showed that the tightened PHSM strategy was associated with successful control of the Omicron variant BA.2 outbreak. Effective transmission was significantly decreased under the restrict strategy, along with spatial-

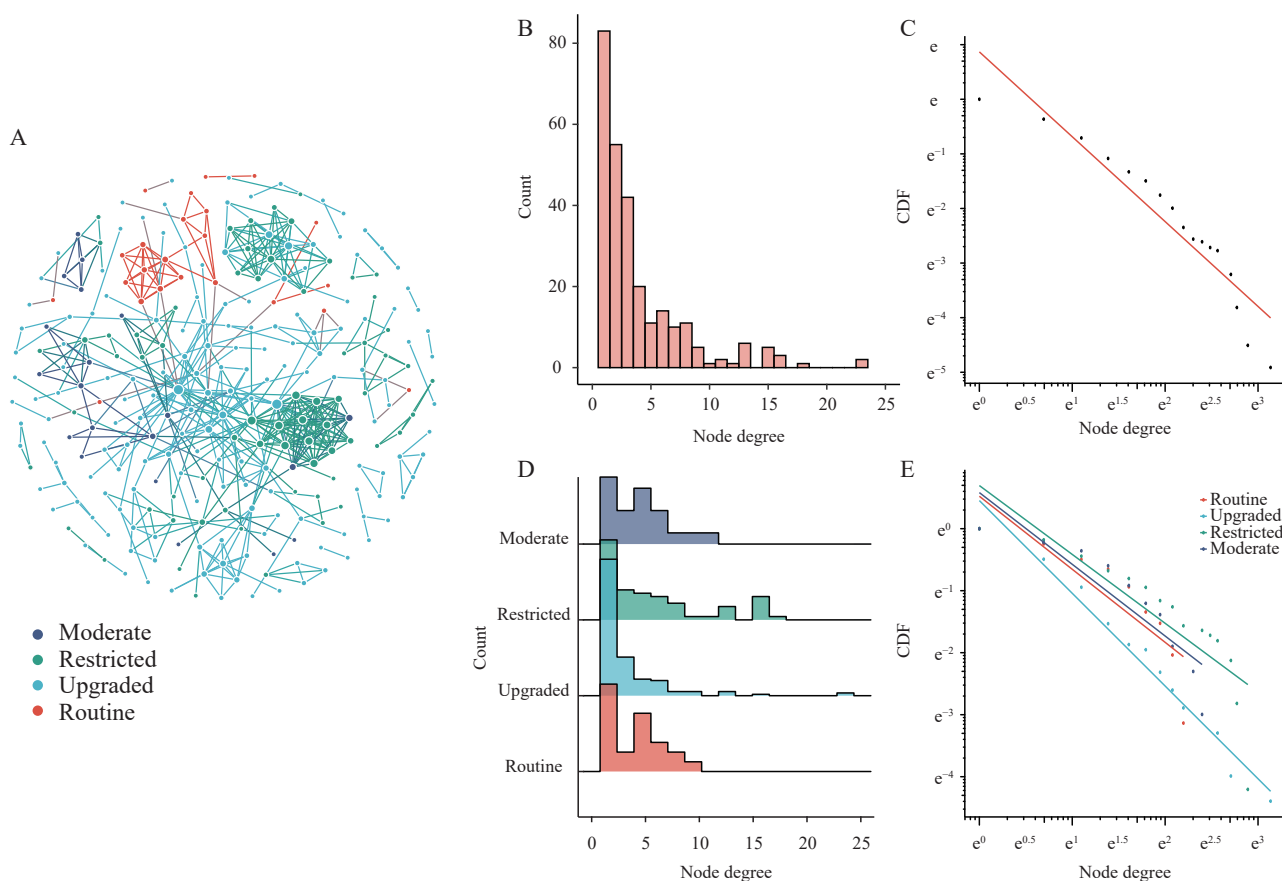


FIGURE 3. The transmission networks and degree distribution of the COVID-19 outbreak in Ruili, China, February–March 2022. (A) The transmission networks of the COVID-19 outbreak. (B) Overall degree distribution of the transmission networks. (C) Overall degree power-law line in the log-log plot. (D) Strategy-stratified degree distribution of the transmission network. (E) Strategy-stratified degree power-law line in the log-log plot.

Note: The transmission network was constructed by 278 confirmed epidemiological links (A). The overall and strategy-specific node degree distribution presented a power-law distribution (B and D). The vital parameter of degree exponent $-\gamma$ was the largest in the upgraded subnetworks (C and E).

Abbreviation: COVID-19=coronavirus disease 2019; CDF=cumulative distribution function.

TABLE 1. Transmission network parameters under public health and social measures strategies in Ruili City, Yunnan Province, China, February–March 2022.

Networks	V	k_{max}	k_{aver}	$-\gamma$	d	l_{aver}	c_{aver}
Overall	272	23	3.86	1.695	9	4.23	0.61
Routine	23	9	3.95	1.692	4	1.90	0.75
Upgraded	162	23	3.02	1.828	9	4.01	0.49
Restricted	67	18	5.68	1.541	5	2.05	0.78
Moderate	20	11	4.40	1.585	3	1.65	0.83

Abbreviation: V=Node; k_{max} =Maximum degree; k_{aver} =Average degree; $-\gamma$ =the degree exponent of power-law distribution; d=Network diameter; l_{aver} =Average path length; c_{aver} =Average clustering coefficient.

temporal clustering limitation and phase transformation of the transmission network. This interdisciplinary exploration helps relevant stakeholders better understand the role of PHSM strategy in responding to the COVID-19 outbreak.

This study characterized the dynamics and key parameters of transmission. The shortened transmission parameter indicated stronger transmissibility of the BA.2 variant. The estimated mean incubation period was 3.6 days (SD=2.1 days) for this Omicron variant BA.2. It was 31% shorter than the primary strain reported in Wuhan (mean=5.2 days) (5), and 18% shorter than the Delta variant B.1.617.2 reported (mean=4.4 days, SD=1.9 days) in Guangzhou, China (6). The mean serial interval was 3.2 days (SD=1.7 days). It was 57% shorter than the primary strain (mean=7.5 days), 6%–16% shorter than that reported in Zhuhai, China (mean=3.4 days, SD=1.7 days) and in the Republic of Korea (mean=3.8 days, SD=3.3 days) compared to Omicron variant BA.1 (7–8). It suggested that more rapid public health measurements should be taken in response to fast spreading variants such as Omicron. The theoretical R_0 was related to the control measures and population immunity level. Although there was a restricted control policy, a 95% population immunity level, and a 92.2% vaccination rate among patients, the R_0 was still slightly larger than 1. It was in line with the estimated $R_0=1.72$ in the Republic of Korea's early Omicron wave, a time when 80% of the population had received 2-dose vaccinations (8). However, a widespread comparison of R_0 should be done cautiously because of varying public health responses and immunity levels.

This study highlighted that transmission was contained after seven days by implementing the most important PHSM of complete in-city travel restriction and region lockdown. The dynamics analysis presented the synchronization of PHSM strategies and R_t . The R_t dramatically decreased by implementing the upgraded and restricted strategies, however, the R_t presented a long tail during the upgraded strategy. The average R_t

among the restricted strategy was 28.4% and 44.8% lower than the routine and upgraded strategy.

Another approach to characterize the effect of different scenarios of interventions is the ordinary differential equations model (ODE), known as the classic Susceptible-Infectious-Recovered (SIR) infectious disease modeling framework. The SIR model designates initial parameters and iterates equations to obtain numerical solutions for different intervention scenarios. The inference of ODE is highly sensitive to initial parameters and is profoundly model-dependent. Dissimilarly, the performed analysis in this study was data-driven by field investigation. Transmission dynamics were based on the nature of disease transmission, including the serial interval and incubation period; thus, the more robust and pragmatic results identified in this study are more beneficial to public health practice than the ODE.

The Knox spatiotemporal interaction analysis allowed this study to examine and identify high strength clusters. The spatiotemporal heterogeneity implied that there was a high risk of COVID-19 infection among nearby spatiotemporal persons. It can be interpreted as showing that a large share of infection and transmission cases were among high-risk close contacts and family clusters.

The quantification of spatial-temporal interaction revealed the impact of PHSM strategies on spatiotemporal clustering. The highest spatial RR was among the routine strategies, and it showed a prolonged RR in the time interval. This implies that the routine strategy could not interrupt long-temporal transmission and short-space infection. The upgraded strategy mitigated short-distance infection compared with the routine strategy, but whole-temporal transmission was higher than the routine. This implies that the implementation of partial in-city travel restriction and risk site lockdowns had an effect on controlling spatial close contact transmission, but temporal risk still could not be suppressed much in extensive community transmission scenarios. The

restricted strategy simultaneously prevented short- and long- transmission in spatiotemporal scale: the transmission was interrupted by implementing a complete in-city travel restriction and region lockdown.

This investigation further found PHSM strategies corresponding to varied patterns of the transmission network. The characteristics and appearance of the transmission network were synchronized with the PHSM strategies. The node degree distribution presented a heavy tail power-law distribution; this was consistent with previous studies in Hong Kong (9). According to the specificity of scale-free networks, the part of the heavy tail of the degree distribution deserves attention. The super-connected nodes were in key positions in the transmission network: identifying super-spreaders in the heavy tail part was thus crucial to controlling the outbreak. Another specificity of the scale-free network was that, if one deletes the most connected node of the network, it would break into many isolated fragments — although the scale-free network showed robustness and tolerance against random failures (10). The topological weakness of transmission networks was due to inhomogeneous power-law connectivity distribution. The network dynamics under different strategies demonstrated the nature of a scale-free network. The most connected nodes, or the super-spreaders, were contained under the restricted strategy; resultantly, the transmission network crashed into many unconnected limited pieces, resulting in a contained outbreak. The perception of phase transformation of complex network dynamics helped deepen the understanding of the PHSM effect on transmission networks.

The epidemiology and dynamics of the outbreak indicated high transmissibility and concealed infectivity of the Omicron variant BA.2. The vital contribution of this study is that it shows evidence that timely PHSMs are essential to control high-risk outbreaks. The timely restricted strategy was sufficient to control COVID-19 even during extensive community transmission scenarios.

The study was subject to at least two limitations. First, there was a high proportion of asymptomatic cases in the outbreak. The fact that the date of the positive test replaced symptom onset for parameter estimation introduces bias. Second, the cases' home addresses were used in the spatial-temporal analysis; thus, it could not consider working locations or public places, and the trajectory and infection exposure might be different in those locations. As such, future studies should address the specific PHSM's impacts on

transmission patterns.

Acknowledgments: Staff of Yunnan CDC, Dehong CDC, Ruili CDC, community health workers, citizens and all those who made tireless contribution to control the outbreak of COVID-19 in Ruili city, Xiaoqing Fu, Juanjuan Li, Yang Chen, Diexin Wei, Jianping Cun, Jinkun Wang, Ying Shao.

Funding: Supported by the Yunnan health training project of high level talents (H-2019027) and Yunnan Provincial High-Level Talent Incubator Program.

doi: 10.46234/ccdcw2022.208

* Corresponding authors: Lin Xu, xulinth@hotmail.com; Manhong Jia, jiaman hong@yncdc.cn.

¹ Yunnan Center for Disease Control and Prevention, Kunming City, Yunnan Province, China.

Submitted: June 05, 2022; Accepted: September 28, 2022

REFERENCES

1. Khandia R, Singhal S, Alqahtani T, Kamal MA, El-Shall NA, Nainu F, et al. Emergence of SARS-CoV-2 Omicron (B. 1.1.529) variant, salient features, high global health concerns and strategies to counter it amid ongoing COVID-19 pandemic. *Environ Res* 2022;209:112816. <http://dx.doi.org/10.1016/j.envres.2022.112816>.
2. Jiang Y, Wu Q, Song PP, You CG. The variation of SARS-CoV-2 and advanced research on current vaccines. *Front Med* 2022;8:806641. <http://dx.doi.org/10.3389/fmed.2021.806641>.
3. Karim SSA, Karim QA. Omicron SARS-CoV-2 variant: a new chapter in the COVID-19 pandemic. *Lancet* 2021;398(10317):2126 – 8. [http://dx.doi.org/10.1016/S0140-6736\(21\)02758-6](http://dx.doi.org/10.1016/S0140-6736(21)02758-6).
4. Yan XY, Chang LT, Wang ZK, Hao LH, Jia ZW, Zhang B, et al. Exploring the bridge cases' role in the transmission of the SARS-CoV-2 delta variant — Ruili city, Yunnan province, China, July–September 2021. *China CDC Wkly* 2021;3(50):1065 – 70. <http://dx.doi.org/10.46234/ccdcw2021.239>.
5. Li Q, Guan XH, Wu P, Wang XY, Zhou L, Tong YQ, et al. Early transmission dynamics in Wuhan, China, of novel coronavirus-infected pneumonia. *N Engl J Med* 2020;382(13):1199 – 207. <http://dx.doi.org/10.1056/NEJMoa2001316>.
6. Zhang M, Xiao JP, Deng AP, Zhang YT, Zhuang YL, Hu T, et al. Transmission dynamics of an outbreak of the COVID-19 Delta variant B.1.617.2 — Guangdong province, China, May–June 2021. *China CDC Wkly* 2021;3(27):584–6. <http://dx.doi.org/10.46234/ccdcw2021.148>.
7. Ruan F, Zhang X, Xiao S, Ni X, Yin X, Ye Z, et al. An outbreak of the COVID-19 Omicron variant — Zhuhai city, Guangdong province, China, January 13, 2022. *China CDC Wkly* 2022;4(30):669 – 71. <http://dx.doi.org/10.46234/ccdcw2022.032>.
8. Kim D, Ali ST, Kim S, Jo J, Lim JS, Lee S, et al. Estimation of serial interval and reproduction number to quantify the transmissibility of SARS-CoV-2 Omicron variant in South Korea. *Viruses* 2022;14(3):533. <http://dx.doi.org/10.3390/v14030533>.
9. Liu Y, Gu ZL, Liu JM. Uncovering transmission patterns of COVID-19 outbreaks: A region-wide comprehensive retrospective study in Hong Kong. *eClinicalMedicine* 2021;36:100929. <http://dx.doi.org/10.1016/j.eclinm.2021.100929>.
10. Albert R, Jeong H, Barabási AL. Error and attack tolerance of complex networks. *Nature* 2000;406(6794):378 – 82. <http://dx.doi.org/10.1038/35019019>.

SUPPLEMENTARY MATERIALS

Study Settings

The study field in Ruili was in Dehong Dai and the Jingpo Autonomous Prefecture of Yunnan Province, located in southwestern China. The area was 944.75 square kilometers, and the resident population was 235,009. Ruili borders Myanmar in the northwest, southwest, and southeast.

The Spatial-temporal Interaction and Risk Evaluation

The spatiotemporal interaction statistic X was constructed and calculated as:

$$X = \sum_{i=1}^n \sum_{j=1}^n a_{ij}^s a_{ij}^t$$

where n is the number of infected cases, a_{ij}^s is the spatial adjacency between i and j case; a_{ij}^s equal to 1 if the distance between i and j less than δ and 0 otherwise. Similarly, a_{ij}^t is the temporal adjacency between i and j case; a_{ij}^t equal to 1 if the distance between i and j less than τ and 0 otherwise. The presupposed δ was the spatial distance threshold, and τ was the temporal interval threshold to define the neighborhood. The Monte Carlo simulation (MCS) was used for the calculation of null distribution of X and the statistic test. MCS randomly permuted a_{ij}^t and kept a_{ij}^s unchanged to estimate the significance under the null hypothesis of no clustering. MCS provided a relative risk (RR) calculation based on the comparison of observed (A_X) and expected (E_X) values of X ,

$$RR = \frac{A_X}{E_X}$$

and the calculation of clustering strength (S),

$$S = \frac{(A_X - E_X)}{E_X} \times 100$$

The epidemiological perception of RR and S was contagiousness and infectivity in spatial-temporal proximity.

SUPPLEMENTARY TABLE S1. The demographic and epidemiological characteristics of COVID-19 cases under public health and social measures strategies in Ruili City, China, February–March 2022.

Characteristics	Overall	Public health and social measures strategies N (%)			
	N (%)	Routine	Upgraded	Restricted	Moderate
	387	40 (10.3)	238 (61.5)	89 (23.0)	20 (5.2)
Gender					
Male	179 (46.3)	19 (47.5)	106 (44.5)	43 (48.3)	11 (55.0)
Female	208 (53.7)	21 (52.5)	132 (55.5)	46 (51.7)	9 (45.0)
Age (years)					
Mean (SD)	34.7 (18.3)	35.0 (17.8)	34.5 (17.4)	33.0 (19.7)	44.3 (20.8)
<15	66 (17.1)	4 (10.0)	40 (16.8)	19 (21.3)	3 (15.0)
15–39	179 (46.3)	25 (62.5)	107 (45.0)	42 (47.2)	5 (25.0)
40–64	117 (30.2)	8 (20.0)	80 (33.6)	21 (23.6)	8 (40.0)
≥65	25 (6.5)	3 (7.5)	11 (4.6)	7 (7.9)	4 (20.0)
Type of case					
Confirmed	70 (18.1)	16 (40.0)	38 (16.0)	14 (15.7)	2 (10.0)
Asymptomatic	317 (81.9)	24 (60.0)	200 (84.0)	75 (84.3)	18 (90.0)
Vaccination					
Vaccinated	357 (92.2)	38 (95.0)	222 (93.3)	79 (88.8)	18 (90.0)
None	30 (7.8)	2 (5.0)	16 (6.7)	10 (11.2)	2 (10.0)

Abbreviation: SD=standard deviation.

Based on the transmission dynamic analysis, this study scanned the spatial-temporal interaction on a scale of spatial distance δ from 0 meters to 5 kilometers (δ was divided into 50 fractions by step size of 100 meters), and a time interval τ from 1 day to 10 days (τ was divided into 10 fractions by step size of 1 day).

The Transmission Networks Analysis

The graphic measurements of the COVID-19 transmission network were defined as:

1. the degree of node (k), the number of connections of a node to other nodes;
2. the maximum degree (k_{max}), the largest value among all nodes' degrees;
3. the average degree (k_{aver}), the mean value of all nodes' degrees;
4. degree distribution: the probability $P(k)$ of a randomly selected node having a degree k in network;
5. the degree exponent of power-law distribution ($-\gamma$), estimated degree distribution of power-law distribution $P(k) \sim k^{-\gamma}$, where the $-\gamma$ is the degree exponent;
6. network diameter (d), the number of edges in the largest path for two connected nodes;
7. average path length (l_{aver}), the average number of edges in the shortest connecting path;
8. average clustering coefficient (c_{aver}), the average probability that two neighbors of a node are also neighbors of each other.

Outbreak Reports

An Outbreak of SARS-CoV-2 Omicron Subvariant BA.2.76 in an Outdoor Park — Chongqing Municipality, China, August 2022

Li Qi¹; Wenge Tang¹; Ju Wang¹; Yu Xiong¹; Yi Yuan¹; Baisong Li¹; Lin Yang¹;
Tingting Li¹; Lianjian Yang²; Xiaoyuan Su³; Qin Li^{1,4}; Lijie Zhang^{4,5}

Summary

What is already known about this topic?

Severe acute respiratory syndrome coronavirus 2 (SARS-CoV-2) Omicron subvariant has a stronger transmission capacity and faster transmission speed than the previous strain.

What is added by this report?

The first coronavirus disease 2019 (COVID-19) case infected with the SARS-CoV-2 Omicron subvariant BA.2.76 who caused local transmission was reported in Chongqing Municipality on August 16, 2022. For 35 minutes, the Patient Zero jogged along a lake at a local park without wearing a mask. Among the 2,836 people potentially exposed at the time, 39 tested positive. Overall, 38 out of 39 cases did not wear a mask on the morning of August 16. All 39 cases lacked any previous exposure to the variant before testing positive on their nucleic acid test.

What are the implications for public health practice?

It is essential to maintain personal wellbeing by ensuring one maintains personal protection and follows regulated guidelines such as maintaining safe distances from others both indoors and outdoors.

The first coronavirus disease 2019 (COVID-19) case infected with the severe acute respiratory syndrome coronavirus 2 (SARS-CoV-2) Omicron subvariant BA.2.76 causing local transmission was reported in Chongqing Municipality on August 16, 2022. For 35 minutes, Patient Zero jogged along a lake in a park without wearing a mask. Of the 2,836 people potentially exposed in the park, 39 tested SARS-CoV-2 positive. Gene analysis from the 39 cases showed highly homologous when compared to Patient Zero. Epidemiological investigations supported that Patient Zero transmitted to the following 33 visitors and 2 park cleaners and the 2 cleaners transmitted to 4 colleagues. This outbreak indicated that the Omicron subvariant BA.2.76 could be easily transmitted to

others outdoors if they are not equipped with effective protection equipment. The public should be encouraged to use good protection measures and retain safe distances amongst others both indoors and outdoors.

INVESTIGATION AND RESULTS

A 41-year-old male COVID-19 case (Patient Zero) was reported in Chongqing on August 16, 2022. He flew to Hohhot City on August 11 and flew back to Chongqing on flight CZ2752 on August 13, 2022. On August 12, this plane was from Chongqing to Hohhot (CZ2751), it housed 4 passengers from Tibet who tested positive for SARS-CoV-2 once they arrived at Hohhot. The flight arriving in Hohhot at 20:00 was not disinfected for the following day's departure for Chongqing (CZ2752) at 09:59 on August 13. Patient Zero took flight CZ2752 and his seat (33K) happened to be situated around the seats of the 3 positive passengers (34A, 34C, 34H) (CZ2751). Case interviewing found that Patient Zero has no epidemiological association with previous cases in Chongqing. All the 40 persons he contacted in Hohhot had negative testing results for SARS-CoV-2 nucleic acid.

The genome sequence analysis conducted by Chongqing CDC showed Patient Zero infected with Omicron BA.2.76, with the same 75 nucleotide mutations as strains from recent local cases in Tibet. The genetic sequences were highly homologous between Patient Zero and the 4 infected passengers in flight CZ2751, which suggested they might belong to a same transmission chain. Patient Zero was infected most likely because of the exposure to contaminated airline environments.

Patient Zero participated in screening for SARS-CoV-2 virus by using community PCR testing sites in Chongqing on August 9, 10, 11, 13, and 14 and results were negative. There was no screening test on August 12 when Patient Zero was in Hohhot. On

August 15, his throat swab specimen was taken at 21:39 and sent to a Medical Laboratory. The positive test result was available at 08:00 on August 16 with ORF lab/N gene: 29.19/31.86. At this time, he just came back home after jogging in the park. He was informed to stay at home and resampled at 09:45, and this result was positive with lower Ct value (ORF lab/N: 19.23/16.96) tested by local CDC.

Local CDC identified close contacts and at-risk populations by case interviewing, review of surveillance footage and action track positioning. Close contacts were persons who have a distance of less than 1 meter with Patient Zero and without effective prevention measures. At-risk populations were persons who had been to areas that Patient Zero visited while without close contact with Patient Zero. Close contacts were quarantined at hotels for 7 days and at-risk populations were quarantined at home for 3 days. Finally, 256 close contacts and 20,496 at-risk populations were identified. Health personnel took daily throat swab for SARS-CoV-2 nucleic acid PCR tests for them.

Among those close contacts and at-risk populations, 48 were infected. Overall, 9 of the 48 individuals were exposed to Patient Zero on August 15 or 16 before Patient Zero jogged, including Patient Zero's wife, 4 colleagues, 2 foot massage therapists, 1 breakfast server, and 1 person on the road. The other 39 cases all had the same exposure of being in the park where Patient Zero jogged on August 16, including 33 visitors and 6 park staff (4 cleaners, 1 lawn mower and 1 park officer). None of the 39 cases were exposed to other previous reported cases or traveled to regions with COVID-19 cases. The 39 cases had positive test throat swabs or developed symptoms between August 17 and 22. The epi curve indicated a point source exposure for 33 visitor cases and the first 2 park cleaner cases (Figure 1). Among the 39 cases, 29 had the exact same gene sequencing as Patient Zero; 5 cases had a mutation site added to Patient Zero's gene sequence; and the other 5 cases could not be sequenced because of unqualified specimens.

The investigation team highly suspected that Patient Zero was the source of this outbreak due to his maskless jogging in the park. Investigators focused on the activities in the park for both Patient Zero and the 39 cases. The park is a cultural park of 42.5 acres. On August 16, Patient Zero entered the park through the east gate at 6:54 am, jogged counterclockwise to the lake and circled the lake 4 times. He left the park along the same roads at the east gate at 07:29. The path

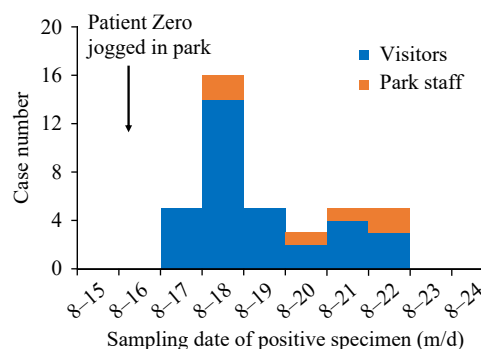


FIGURE 1. The distribution of sampling date for positive specimen in the outbreak of severe acute respiratory syndrome coronavirus 2 Omicron subvariant BA.2.76 in an outdoor park in Chongqing Municipality, China, August 2022.

Note: Two cases developed symptoms earlier than the positive specimen date, their onset dates were used in the epi curve.

width of jogging was about 4 meters. The wind speed was 0.5–3.0 m/s, the temperatures were 33.0°C–42°C and the air humidity was 44%–48% when Patient Zero was jogging. The east gate of the park is the main gate, with convenient transportation, and a good flow of people. During the jogging time, there were 104 close contacts who have a distance less than 1 meter with Patient Zero and without wearing masks.

Patient Zero felt fatigue on August 15 but had no symptoms of fever or cough. He did not wear a mask during his jogging in the park. He did not use any facilities and interact with others in the park. Among the 33 cases among visitors, 13 were close contacts who had faced with or passed by Patient Zero when they exercised by reviewing surveillance footage in the park, 20 were at risk due to exposure to Patient Zero. Among the 20 at-risk populations, 10 cases had both stayed for a while around the lake and entered the park through the same east gate as Patient Zero, 2 cases stayed around the lake, 1 case entered the park through east gate, the other 7 cases had neither stayed around the lake nor entered the park through east gate, but part of their walking routes in the park overlapped with the route Patient Zero had taken. The 33 visitor cases did not know each other, no COVID-19 cases in the communities where they dwelled and no time-space overlap with previous reported COVID-19 cases before they tested positive.

There were 24 staff in the park. From August 18 to 20, they worked in the park during the day and rested in two big meeting rooms at night until they were transferred to quarantine hotels. During the 3 days, they shared the same toilet. Two park cleaners who

worked in the area of the lake tested positive on August 18, then the other 4 park staff subsequently tested positive on August 20 (1 case), 21 (1 case), and 22 (2 cases). It was possible that the first 2 cleaner cases infected the other 4 staff during the 3 days.

DISCUSSION

This investigation reported a male infected with Omicron BA.2.76 subsequently infecting 33 visitors and 2 park cleaners while he jogged in a park. Neither Patient Zero nor the 33 visitors wore masks when they visited the park.

The risk of virus transmission in outdoor locations has been lower than in indoor spaces (1). Literature had reported several SARS-CoV-2 infections and outbreaks occurred outdoors (2–5). However, these reports do not exclude the possibility of direct contact to cases in indoor spaces. In this outbreak, the only possible exposure for the 33 visitor cases and 2 park cleaner cases were in the park at the same time as Patient Zero. Both epidemiological investigation and gene sequence analysis supported the findings of SARS-CoV-2 infections occurred in the park during Patient Zero jogged. This transmission occurred in the park without directly contacting others.

Literature showed that factors which could affect outdoor transmission of SARS-CoV-2 included duration of exposure, frequency of exposure, density of gathering, sunlight, temperature (6), air humidity (7), and use of masks, etc. The BA.2.76 and BA.2.75 strains of Omicron are growing rapidly in India, showing priority compared with other lineages (8). In this outbreak, the throat swab specimen of Patient Zero was positive for COVID-19 virus nucleic acid test on August 15. Patient Zero developed symptoms of fatigue the day before his jogging. When Patient Zero jogged, the transmission of the virus increased due to the excessive heavy breathing. A study applied a model and claimed that runners, who in their exercise state produce stronger inhalation and exhalation breaths, could be more prone to being infected with COVID-19 (9). The 33 visitor cases who had morning exercises in the park had higher opportunities to be infected. They could quickly encounter particles in the air that might contain the virus because of the stronger breath during exercises (10). In addition, turbulent airflow generated by intense physical exercise might be the cause of more dense transmission (11–12). In our report, Patient Zero jogged for 35 minutes, it is

reasonable to assume that he may have emitted an abundance of virus-laden respiratory particles and spread SARS-CoV-2.

There were limitations in this investigation. First, for some cases in visitors, we could not find the exact contact situation with Patient Zero because of limited surveillance footage in the park. The second is that 5 cases were not sequenced because of low-quality specimens.

Personal protection measures including maintaining social distance and wearing masks were the most effective ways to prevent transmission and infection (1). This investigation showed Patient Zero and the 35 subsequent infected individuals did not wear masks when they were in the park. Only the park officer case wore a mask when he worked. Thus, this led to the transmission of SARS-CoV-2. Although some scholars pointed out that wearing a mask during exercise will cause great resistance to breathing (13), given the stronger transmission capacity and faster transmission speed of Omicron subvariant, the public should be encouraged to use good personal protection measures during the COVID-19 epidemic even while outdoors.

In conclusion, this outbreak showed that a COVID-19 case infected with Omicron subvariant BA.2.76 transmitted to 33 visitor cases and 2 park working staff in an outdoor park when the first case jogged. It was highly possible SARS-CoV-2 transmission could easily occur outdoors if effective prevention was not taken. Therefore, physical distancing and correct use of masks should be emphasized as important strategies for mitigating transmission in congregate settings. In the current Dynamic COVID-Zero Policy in China, keeping good personal protection and maintaining safe distances should be strongly recommended not only indoors, but also outdoors.

Acknowledgements: The Staff members at Shapingba, Changshou, Qijiang, Yubei CDCs and the investigation subjects.

Conflicts of interest: No conflicts of interest.

Funding: Supported by Chongqing Science and Technology Bureau (CSTC2021jscx-gksb-N0005).

doi: 10.46234/ccdcw2022.209

Corresponding authors: Qin Li, 503568313@qq.com; Lijie Zhang, zhanglj@chinacdc.cn.

¹ Chongqing Center for Disease Control and Prevention, Chongqing Municipality, China; ² Shapingba Center for Disease Control and Prevention, Chongqing Municipality, China; ³ Yubei Center for Disease Control and Prevention, Chongqing Municipality, China; ⁴ Chinese Center for Disease Control and Prevention, Beijing, China.

Submitted: October 22, 2022; Accepted: November 16, 2022

REFERENCES

1. Bulfone TC, Malekinejad M, Rutherford GW, Razani N. Outdoor transmission of SARS-CoV-2 and other respiratory viruses: a systematic review. *J Infect Dis* 2021;223(4):550 – 61. <http://dx.doi.org/10.1093/infdis/jiaa742>.
2. Szablewski CM, Chang KT, Brown MM, Chu VT, Yousaf AR, Anyalechi N, et al. SARS-CoV-2 transmission and infection among attendees of an overnight camp - Georgia, June 2020. *MMWR Morb Mortal Wkly Rep* 2020;69(31):1023 – 5. <http://dx.doi.org/10.15585/mmwr.mm6931e1>.
3. Leclerc QJ, Fuller NM, Knight LE, CMMID COVID-19 Working Group, Funk S, Knight GM. What settings have been linked to SARS-CoV-2 transmission clusters? *Wellcome Open Res* 2020;5:83. <http://dx.doi.org/10.12688/wellcomeopenres.15889.2>.
4. Qian H, Miao T, Liu L, Zheng XH, Luo DT, Li YG. Indoor transmission of SARS-CoV-2. *Indoor Air* 2021;31(3):639 – 45. <http://dx.doi.org/10.1111/ina.12766>.
5. Sky News. Coronavirus: champions League match a 'biological bomb' that infected Bergamo, experts say. 2020. <https://news.sky.com/story/coronavirus-champions-league-match-a-biological-bomb-that-infected-bergamio-experts-say-11963905>. [2022-10-2].
6. Ran X, Hazhir R, Marichi G, Catherine Di, Navid G, Heresh A et al. Weather, air pollution, and SARS-CoV-2 transmission: a global analysis. *Lancet Planet Health* 2021;5(10):e671 – e680. [http://dx.doi.org/10.1016/S2542-5196\(21\)00202-3](http://dx.doi.org/10.1016/S2542-5196(21)00202-3).
7. Skanata A, Spagnolo F, Metz M, Smyth DS, Dennehy JJ. Humidity reduces rapid and distant airborne dispersal of viable viral particles in classroom settings. *Environ Sci Technol Lett* 2022;9(7):632 – 7. <http://dx.doi.org/10.1021/acs.estlett.2c00243>.
8. Cao YL, Song WL, Wang L, Liu P, Yue C, Jian FC, et al. Characterization of the enhanced infectivity and antibody evasion of Omicron BA. 2.75. *Cell Host Microbe* 2022;30(11):1527 – 39.e5. <http://dx.doi.org/10.1016/J.CHOM.2022.09.018>.
9. Arias FJ. Are runners more prone to become infected with COVID-19? An approach from the raindrop collisional model. *J Sci Sport Exerc* 2021;3(2):167 – 70. <http://dx.doi.org/10.1007/s42978-020-00071-4>.
10. Klompas M, Milton DK, Rhee C, Baker MA, Leekha S. Current insights into respiratory virus transmission and potential implications for infection control programs: a narrative review. *Ann Intern Med* 2021;174(12):1710 – 8. <http://dx.doi.org/10.7326/M21-2780>.
11. Atrubin D, Wiese M, Bohinc B. An outbreak of COVID-19 associated with a recreational hockey game - Florida, June 2020. *MMWR Morb Mortal Wkly Rep* 2020;69(41):1492 – 3. <http://dx.doi.org/10.15585/mmwr.mm6941a4>.
12. Majra D, Benson J, Pitts J, Stebbing J. SARS-CoV-2 (COVID-19) superspreader events. *J Infect* 2021;82(1):36 – 40. <http://dx.doi.org/10.1016/j.jinf.2020.11.021>.
13. Poon ETC, Zheng C, Wong SHS. Effect of wearing surgical face masks during exercise: does intensity matter? *Front Physiol* 2021;12:775750. <http://dx.doi.org/10.3389/fphys.2021.775750>.

Indexed by PubMed Central (PMC), Emerging Sources Citation Index (ESCI), Scopus, Chinese Scientific and Technical Papers and Citations, and Chinese Science Citation Database (CSCD)

Copyright © 2022 by Chinese Center for Disease Control and Prevention

All Rights Reserved. No part of the publication may be reproduced, stored in a retrieval system, or transmitted in any form or by any means, electronic, mechanical, photocopying, recording, or otherwise without the prior permission of *CCDC Weekly*. Authors are required to grant *CCDC Weekly* an exclusive license to publish.

All material in *CCDC Weekly Series* is in the public domain and may be used and reprinted without permission; citation to source, however, is appreciated.

References to non-China-CDC sites on the Internet are provided as a service to *CCDC Weekly* readers and do not constitute or imply endorsement of these organizations or their programs by China CDC or National Health Commission of the People's Republic of China. China CDC is not responsible for the content of non-China-CDC sites.

The inauguration of *China CDC Weekly* is in part supported by Project for Enhancing International Impact of China STM Journals Category D (PIIJ2-D-04-(2018)) of China Association for Science and Technology (CAST).



Vol. 4 No. 46 Nov. 18, 2022

Responsible Authority

National Health Commission of the People's Republic of China

Sponsor

Chinese Center for Disease Control and Prevention

Editing and Publishing

China CDC Weekly Editorial Office
No.155 Changbai Road, Changping District, Beijing, China
Tel: 86-10-63150501, 63150701
Email: weekly@chinacdc.cn

CSSN

ISSN 2096-7071
CN 10-1629/R1